博士論文

論文題目

Investigation and clinical application of contrast enhanced magnetic resonance digital subtraction angiography (MRDSA)

（磁気共鳴デジタル差分血管造影法（MRDSA）の研究）

Harushi Mori

森　墾

博士論文

論文題目

Investigation and clinical application of contrast enhanced magnetic resonance digital subtraction angiography (MRDSA)

（磁気共鳴デジタル差分血管造影法（MRDSA）の研究）

Supervisor: Professor Kuni Ohtomo

指導教員：大友　邦　教授

Harushi Mori

森　墾

Department of Radiology
Graduate and Faculty of Medicine
The University of Tokyo

東京大学大学院医学系研究科　生体物理医学専攻　放射線医学講座

1. Table of Contents

2. List of Abbreviations and Acronyms

ACA	anterior cerebral artery
ASSET	array spatial sensitivity encoding techniques
AVM	arteriovenous malformation
BA	basilar artery
CE	contrast enhanced
CNR	contrast to noise ratio
DSA	digital subtraction angiography
FA	flip angle
FOV	field of view
Gd	gadolinium
GE	gradient echo
IADSA	intraarterial digital subtraction angiography
ICA	internal carotid artery
IVMR	interventional MR
MCA	middle cerebral artery
MIP	maximum intensity projection
MRA	magnetic resonance angiography
MRDSA	magnetic resonance digital subtraction angiography
MRI	magnetic resonance imaging
NEX	number of excitation
PCA	posterior cerebral artery
PC-MRA	phase-contrast magnetic resonance angiography

RF	radiofrequency
SI	signal intensity
SNR	signal to noise ratio
SPGR	spoiled gradient recalled echo
SSR	signal of brain to signal of contrast agent ratio
SSS	superior sagittal sinus
T	Tesla
TE	echo time
TOF-MRA	time-of-flight magnetic resonance angiography
TR	repetition time
TRICKS	time-resolved imaging of contrast kinetics
VA	vertebral artery

3. List of Publications

Permissions are granted for me to use all the articles for my doctoral thesis and to e-publish them at the UTokyo repository.

1. Mori H, Aoki S, Okubo T, Hayashi N, Masumoto T, Yoshikawa T, Tago M, Shin M, Kurita H, Abe O, Ohtomo K.
Two-dimensional thick-slice magnetic resonance digital subtraction angiography in the assessment of intracranial small- to medium-sized arteriovenous malformations.
Neuroradiology. 2003; 45(1):27-33. → Part 2
The final publication is available at Springer via http://dx.doi.org/10.1007/s00234-002-0844-5

2. Mori H, Aoki S, Masumoto T, Yoshikawa T, Tago M, Shin M, Ohtomo K, Kabasawa H.
Two-dimensional magnetic resonance digital subtraction angiography using array spatial sensitivity encoding techniques in the assessment of intracranial hemodynamics.
Radiat Med. 2002; 20(5):223-229. → Part 3

3. Kunishima K, Mori H, Itoh D, Aoki S, Kabasawa H, Koga T, Maruyama K, Masumoto T, Abe O, Ohtomo K.
Assessment of arteriovenous malformations with 3-Tesla time-resolved, contrast-enhanced, three-dimensional magnetic resonance angiography.
J Neurosurg. 2009; 110(3):492-499. → Part 4
The final publication is available at American Association of Neurological Surgeons via http://dx.doi.org/10.3171/2008.7.JNS08173

4. Research Background

Recent advances in magnetic resonance imaging (MRI) software and hardware have made specialized imaging methods possible for a variety of clinical objectives. Advances in MR angiography (MRA) have been particularly noteworthy, and MRA is now available at many institutions. Standard MRA techniques such as time-of-flight MRA (TOF-MRA) and phase-contrast MRA (PC-MRA) yield superior spatial resolution, but several problems remain (6, 13, 38, 41, 65, 76). Intravascular turbulence and the accompanying spin dephasing that can occur in areas of vascular bifurcation, stenosis, and dilation cause signals to decrease (76). Moreover, imaging times are around 10 minutes, and the degree of temporal resolution is low; thus, almost no information on hemodynamics can be obtained. The reasons for this are outlined below.

TOF-MRA is a widely used form of MRA that makes use of the inflow effect, in which blood flowing into the imaging plane exhibits high signal intensity. However,

capturing the inflow effect requires a large number of adjustments to ensure that blood flow is as nearly perpendicular to the cross section as possible. This, combined with the requirement for thin cross sections, results in long imaging times.

PC-MRA detects the changes in the transverse magnetic phase of protons in the imaging plane (phase shift) that accompany motion within the gradient magnetic field to yield information on phases within the flow encode gradient. By varying the size of this gradient, flows of different velocities can be depicted, allowing differentiation of arteries and veins. However, to capture blood flow over a wide area, it is basically necessary to gather phase shift values for 3 separate images, i.e., along the x, y, and z axes, which is a drawback because this step inevitably lengthens the imaging times. Moreover, the size of the flow encode gradient must be determined in advance based on the predicted blood flow velocity. If this value is not appropriate, the exam will not yield accurate information. For example, while it is known that children have a greater

cerebral blood flow velocity than adults, it can be difficult to accurately predict the degree of this difference. In addition, PC-MRA offers poorer depiction than TOF-MRA in areas of turbulence.

A major advantage of both TOF-MRA and PC-MRA is that these methods do not require contrast agents and can thus depict the vascular lumen noninvasively. However, there are 3D contrast MRA techniques that have been devised to utilize the T1-shortening effect of gadolinium (Gd) chelate MRI contrast agents to obtain angiograms (4, 27, 29, 36, 51, 52, 55, 57, 59, 60, 61, 77, 78, 79). In the past, excessive artifacts and other issues made acquisition of good-quality images difficult, but advances in MR hardware and software, including newer high-speed imaging methods and high-quality coils, have rapidly expanded the clinical use of 3D contrast MRA. Since this method does not use the inflow effect and obtains angiograms through the T1-shortening effect of the contrast agent, the results are not easily

influenced by the speed and direction of blood flow, turbulence, or other such issues encountered with MRA that relies on the inflow effect, including failure to detect areas of vascular stenosis and difficulty distinguishing blockages. Moreover, the images produced by 3D contrast MRA are similar to those obtained using conventional iodine contrast X-ray angiography, making interpretation relatively easy (39). To date, these advantages have mostly been applicable to MRA for the thoracic and abdominal aorta, pelvis, and legs because it is currently not possible to maintain sufficient spatial resolution with 3D contrast MRA when imaging at less than 3 seconds per phase, even with the most technologically advanced MR equipment. Because of this, 3D contrast MRA has been unsuitable for short intracranial circulation times (18, 26, 33). Acquiring hemodynamic information on cranial lesions, particularly cerebrovascular disorders involving arteriovenous malformations (AVM) and fistulas, requires a temporal resolution of at least 1 second per phase (10, 30, 46). Moreover, as

hemodynamics plays an extremely important role in diagnosing certain lesions such as cerebrovascular occlusions, vascular malformation, etc. (28, 48), it is necessary to be able to differentiate arterial and venous phases. Several authors have reported attempts to use 2D or projective contrast MRA in the limbs and trunk (1, 14, 26, 35, 71), but despite some increase in speed, there have been no reports on attempts to use 2D contrast MRA in assessments of the head.

To address this, I have devised a contrast MR digital subtraction angiography technique (MRDSA, **Appendix 1**) that uses 2D imaging and an MRI contrast agent (Gd chelate) with the objective of greatly improving temporal resolution and allowing visualization of blood vessels in a manner similar to that achieved with regular conventional X-ray digital subtraction angiography (intraarterial DSA, IADSA). I established and tested basic imaging parameters, examined clinical applications for intracranial imaging, and investigated methods of increasing speed and providing

3-dimensionalization.

Specifically, the steps in my investigation of the potential clinical application of MRDSA were as follows:

In Part 1, basic experiments were performed using several parameters to optimize the pulse sequence for MRDSA imaging.

In Part 2, MRDSA was tested clinically in cases of cranial AVM. The images produced with MRDSA were compared to those obtained by conventional angiography to determine whether MRDSA could be a useful alternative to repeated angiographies during the post-gamma knife observation period.

In Part 3, I applied parallel imaging technology, which is a high-speed imaging method, to MRDSA to investigate whether improved temporal resolution would assist the clinical evaluation of intracranial blood vessels.

In Part 4, evaluations of cerebral AVMs by X-ray IADSA and contrast-enhanced

MRDSA 3-dimensionalized with time-resolved imaging of contrast kinetics (TRICKS) were compared, and the usefulness of each technique examined. I employed TRICKS sequence instead of stereoscopic 2D-SPGR because of the abundance of 3D information with TRICKS over SPGR. Thus, this part was not actually reflected the results of the Part1. I fixed the optimum TRICKS imaging parameters according to the previous studies (7, 8, 58).

In all studies, informed consent was obtained from each patient or the patient's guardian in the case of underage patients prior to MRDSA and conventional catheter angiography. That is, I followed standard procedure at the time. Nevertheless, I did not submit these studies to institutional review board and the subsequent permission for the retroscopic imaging studies (IRB No.2561) might scarcely cover these studies.

5. Part 1: Investigation of Optimal Conditions

5-1. 【Introduction】

Recent advances in technology have resulted in a wide range of clinical applications for MRA. However, there are several problems with TOF-MRA and PC-MRA, which are the forms of MRA that many institutions use regularly. These problems include the following: (1) despite possessing superior spatial resolution, imaging ability declines due to signal loss in areas of vascular bifurcation, stenosis, dilation, and flexion; and (2) the techniques cannot yield information on hemodynamics due to their low temporal resolution. Thus, in this study, I have devised a method of 2D Gd chelate contrast-enhanced MRDSA, with the objective of greatly improving temporal resolution and to depict blood vessels with an image quality that is similar to that obtained using conventional X-ray DSA, and have performed basic investigations of this method.

5-2. 【Materials and Methods】

Experiments with the parameters described below were conducted to optimize the imaging pulse sequence for a 1.5 tesla (T) MRI device (Signa Horizon, General Electric, Milwaukee, Wis.; gradient magnetic field intensity, 23 mT/m; slew rate, 120 mT/m/ms). The imaging pulse sequence used spoiled gradient recalled echo (SPGR), which is a high-speed gradient echo imaging method. Echo planar imaging is an ultra high-speed imaging method that is currently possible with high-performance MRI and is being applied clinically, such as in perfusion images. And imaging with SPGR is possible even with low magnetic field devices that lack high-performance gradient magnetic fields. Although its signal-to-noise ratio (SNR) is inferior to imaging performed using high magnetic field devices, SPGR allows MRDSA to be performed on a larger number of devices.

MR images are generated using parameters such as echo time (TE), repetition time (TR), and flip angle (FA). For regular imaging, rough values for these parameters are

determined. The 2D-SPGR method used with MRDSA in the present study has mostly been used for high-speed imaging of post-contrast T1-weighted images in the trunk and limbs. The parameters for these post-contrast studies cannot be considered optimal for contrast imaging with MRDSA. Therefore, my first step was to perform basic examinations of several parameters to optimize the pulse sequence for this imaging method. Basic imaging sequence is as follows.

MRDSA：TR/TE= 6.9/1.9msec, flip angle= 90°, bandwidth= 62.5kHz, FOV= 24×24cm, slice thickness= 50mm, Matrix= 512×192, NEX (number of excitation)= 1.

a. Echo time (TE)

Signal intensity (SI) in 2D-SPGR is expressed by formula [1], below (25).

$$\mathbf{SI = \rho \cdot \{1 - \exp(-TR/T1)\} / \{1 - \cos(\alpha) \cdot \exp(-TR / T1)\} \cdot \sin(\alpha) \cdot \exp}$$

(−TE / T2*) [1]

(ρ = proton density; α = flip angle; T1 and T2* are intrinsic values determined by the substance being imaged)

From formula [1], it is expected that shorter TE (msec) will produce higher ratios of background signal to contrast-filled blood vessels. In other words, shorter TE should theoretically result in better background to blood vessel signal ratios with 2D-SPGR MRDSA because the T1-shortening effect of the MRI contrast agent will create contrast between blood vessels and the background (51). To test this theory, the repetition time (TR) was fixed at 10 msec while TE was varied from 1.7 msec to 5.0 msec while keeping all other parameters fixed. The differences in SI were examined by placing a diluted contrast agent around the heads of volunteers and comparing SI measurements from a region of interest (ROI) of brain tissue with an ROI from the

contrast agent. The SI difference was divided by the standard deviation of the brain tissue to determine the brain signal to contrast agent signal ratio (SSR, so-called SNR). The contrast agent was diluted to a 1:16 concentration, supposing that a maximum dilution concentration of about 1:16 would occur with intravenous injection of the contrast agent at 5 mL/sec and an average cardiac output of about 80 mL/sec.

b. Repetition time (TR)

As demonstrated by SI formula [1], as the TR (msec) is decreased, the SI, which reflects the T1 value, increases. Furthermore, reducing TR also shortens the imaging time. However, reducing TR generally decreases the SNR of the overall image. Here, TE was fixed at 1.7 msec while TR was varied from 6.5 msec to 20 msec and the ratios of blood vessel SI to background SI were calculated by the same methods used in (a).

c. Flip angle (FA)

The spin echo method uses a 90° radiofrequency pulse (RF pulse). However, with the gradient echo method used here, imaging is normally performed at 90° or less, and this is called the flip angle (FA). The FA (α_E; Ernst angle) at which the SI is greatest at given T1 and TR values is generally expressed in formulas such as formula [2].

$$\cos(\alpha_E) = \exp(-TR/T1) \quad [2]$$

However, the optimal FA for one type of tissue is not necessarily best for other tissues. Thus, FA was varied from 10° to 90° and the same methods used in (a) and (b) were employed to determine the ratios of blood vessel SI to background SI.

d. Contrast agent concentration

MRI contrast agents have both a T1-shortening effect and a T2-shortening effect, and therefore contrast agent concentration and SI do not have a linear relationship, and it is necessary to investigate the optimal concentration for each parameter. Thus, a phantom with the contrast agent diluted to several concentrations was created and then imaged with the MRDSA pulse sequences so the SI could be compared.

e. Slice thickness

A characteristic of the proposed imaging method is its use of thick 2D slices. However, it is known that thick slices lead to inaccurate slice profiles in MRI. Thus, to investigate ideal thickness, another phantom (**Fig. 1-1**) was created and MRDSA imaging was performed to compare the SI at different thicknesses.

5-3. 【Results】

a. Echo time (TE)

The SI of the diluted contrast media increased as TE was shortened, while the SI of brain matter remained constant. Thus, the SSR was inversely related to TE (**Fig. 1-2**).

b. Repetition time (TR)

The SI of the diluted contrast media decreased slightly as TR was shortened, while the SI of brain matter decreased greatly. Thus, the SSR was inversely related to TR (**Fig. 1-3**).

c. Flip angle (FA)

The SI of the diluted contrast media decreased markedly as FA declined, and the SI of brain matter increased. Thus, SSR was directly related to the FA (**Fig. 1-4**).

d. Contrast agent concentration

The SI of the contrast agent was highest at a dilution of around 1:8, and decreased with both higher and lower concentrations (**Fig. 1-5**).

e. Slice thickness

The contrast agent SI and the contrast to noise ratio (CNR) decreased as slice thickness increased. The signal decreased gradually even laterally along with slice thickness (**Fig. 1-6**).

5-4. 【Discussion】

The TE and TR results were expected based on the principles of MRI. That is, a contrast agent diluted in anticipation of smaller T1 values due to fat, which is a model of blood vessels injected intravenously with a bolus, has a relatively small TE (3 to 10 ms), and as the TE decreases, the signal value increases. In contrast, the background brain tissues exhibited relatively large T1 values, about 780 msec in white matter and about 920 msec in gray matter, with 1.5 T imaging, and varying TE produced almost no change in SI. Similar results were observed with TR, in that reducing TR was important to shortening imaging times. The first conclusion that can be deduced from the TE and TR results is that making TE as short as possible is tied to an increased SSR.

The second conclusion is that the influence of FA should be considered so as to maximize the SI of the contrast media. This is because with a short TE, the contrast agent has a larger effect on the SSR than does the brain matter.

In the conditions of this experiment, the TE/T2* ratio was sufficiently small (TE << T2*) so as to make it negligible (TE/T2* ≒ 0). Thus, the SI (formula [1]) can be approximated as:

SI ≒ ρ・{1 − exp (−TR/T1)} / {1 − cos (α) ・ exp (−TR / T1)} ・ sin (α) [3].

Further, if exp (−TR / T1) is denoted as E, then formula [3] differentiated for α is:

d (SI) / dα = ρ ・ (1−E) ・ [−2E cos 2 (α) + cos (α) + E / 2 {1 −cos (α) }] [4].

Moreover, the T1 value for the contrast agent inside the blood vessels during MRDSA imaging at 1.5 tesla can be expressed by the formula below (51) (Note: R is the T1 relaxivity of the Gd contrast agent).

1 / T1 = 1 / 1200 + R ・ [Gd] [5]

([Gd] = Gd contrast agent injection rate / cardiac output ≒ concentration; R ＝ about 4.5 $msec^{-1}$ ・ $mmol^{-1}$)

Thus, imaging with a 1.5 tesla device at TR = 6.5 msec and a Gd contrast agent injection rate of 10 mL/sec would result in a T1 value of about 4 msec. E = exp (−TR / T1) ≒ 0.197 at this time, and within the 0 ≦ α ≦ 90° range, the differential formula [4] always returns correct values. That is, the SI formula [3] is at its maximum at α = 90°. This is consistent with the results of the experiment.

The optimization of contrast agent concentration is unnecessary when intravenous MRDSA imaging is performed, but I investigated the topic in anticipation of clinical use of interventional MR (IVMR), which will require intra-arterial MRDSA. Generally,

when undiluted MRI contrast materials are used, the T2-shortening effect will cause the signal to decline. Thus, it is necessary to determine optimal concentrations for intra-arterial administration. My finding that a 1:8 dilution is optimal applies to intravenous imaging and indicated that contrast agents should be injected as quickly as possible at the highest possible volume.

This leaves the discussion of slice thickness. Increasing slice thickness naturally increases the number of protons within each pixel, which necessarily increases the SI. In addition, since the signal is obtained in a state where the blood vessels and background tissue are intermingled in the same pixel, the proportion of intermingled background signals increases as slices become thicker. Accordingly, in my experiment, the signal ratio of vessels filled with contrast to other background elements decreased as slice thickness increased. Thus, slice thickness should be kept to a minimum based on the nature of the lesion, although when capturing an overall image of the emissary

veins, the range ends up being large enough to cover the entire cerebral hemisphere.

Assessment of hemodynamics frequently plays an important role in the diagnosis of intracranial lesions (28, 48). The short circulation time in the brain makes evaluating hemodynamics with conventional CT angiography and MR angiography difficult, and DSA using conventional X-ray examinations often remains the diagnostic tool of choice for the head and neck region. The radiation hazard of X-ray DSA cannot be ignored, particularly as lesions such as AVM or fistula are often seen in young people. Moreover, although reports vary, other complications from repeated X-ray DSA exams are observed in 0.5–1% of cases (24, 34), which means that the invasiveness of the technique itself can be problematic. The advantages of the MRDSA technique proposed here are its relatively low level of invasiveness and the ability to perform repeated exams without risk of X-ray radiation exposure.

Regarding temporal resolution, it is thought that MRDSA could be an extremely

useful supplement to conventional MRA, especially in diseases where temporal resolution is helpful for diagnosis (i.e., AVM, moyamoya disease, etc.). Normally, perfusion-weighted imaging, which utilizes the magnetic effect of the contrast agent, is used in MRI evaluation of characteristics such as the development of collateral circulation (56, 62, 72). Perfusion-weighted imaging can accurately evaluate local hemodynamics and it has been even been reported to be useful for evaluating brain tumors. While there is no need to doubt the utility of perfusion-weighted imaging, it requires high magnetic field machines with high gradient performance, as well as software for postprocessing. Although image processing has become simpler, it is still complex, and interpretation of the resulting images is also challenging. As an alternative, MRDSA offers both simple image creation and easy interpretation. MRDSA images resemble conventional X-ray DSA images and can be said to depict nearly the same information as X-ray DSA.

5-5.【Conclusion】

The benefit of static imaging by MRA and CTA has been well documented, but in many cases, additional information on hemodynamics is required. Moreover, temporal resolution is particularly important in diagnosing cerebrovascular disorders, and contrast MRA of the head and neck region is problematic because the short circulation time causes depicted veins to overlap with arteries. Advances in MR technology have shortened both TR and TE, which has reduced imaging times and made it relatively easy to differentiate arteries and veins. However, it remains difficult to realize 1 slab per second with 3D contrast MRA using existing technology. When temporal resolution is a priority, 2D imaging is currently the more appropriate choice because of the trade-off between temporal and spatial resolution in which prioritizing temporal resolution means sacrificing spatial resolution. Thus, I have adjusted several different conditions to optimize MRDSA imaging.

1. Making TE and TR as short as possible.

2. FA should be 90°.

3. Making concentration of contrast agent as dense as possible (when IV injection).

4. Slice thickness should be kept to a minimum based on the nature of the lesion.

6. Part 2: Clinical Application of Magnetic Resonance Digital Subtraction Angiography to Small- to Medium-Sized Intracranial Arteriovenous Malformations

6-1. 【Introduction】

Intracranial arteriovenous malformations (AVMs) are the underlying cause of a sizable proportion of all strokes, and typically affect otherwise healthy young adults. In many cases, early venous filling during conventional intraarterial digital subtraction angiography (IADSA) may offer the only diagnostic clue in the detection of small AVMs or postoperative, embolized, or irradiated AVMs with slow flow.

Flow-dependent magnetic resonance angiography (MRA) including three-dimensional (3D) time-of-flight (TOF) or 3D phase-contrast (PC) MRA, which afford less hemodynamic information, are useful for detection of AVMs involving abnormalities by indicating feeding vessels, but high temporal resolution imaging is essential for hemodynamic evaluation and may be an alternative to the more invasive IADSA techniques in some cases. A clinical complication rate of 0.5 to 2% has been reported

with IADSA (24), and IADSA has also been associated with a silent embolism rate of up to 23% as confirmed on diffusion-weighted MR imaging (5). Efforts should be undertaken to minimize the frequency of invasive procedures that are relevant to associated diagnostic imaging.

MR angiographic images with display mimicking IADSA can be obtained by combination of a bolus contrast injection, two-dimensional (2D) thick-slice acquisition, and a subtraction technique. This 2D thick-slice magnetic resonance digital subtraction angiography (2D MRDSA) may possess higher temporal resolution than 3D techniques, and moreover, the protocol may provide sufficient hemodynamic data with which to evaluate intracranial AVMs.

Several authors have reported 2D acquisition of contrast-enhanced (CE) MRA (1, 3, 14, 21, 26, 35, 68, 71, 80). Here, I evaluated the clinical applicability of 2D MRDSA in the assessment of intracranial AVM in a group of patients who had undergone AVM

radiosurgery at my institution to determine the accuracy of 2D MRDSA in comparison to IADSA as a method for the evaluation of AVMs following gamma-knife radiosurgery.

6-2. 【Materials and Methods】

Patients

Sixty-seven consecutive patients presenting with treated or untreated intracranial AVMs who were referred to my institution for 2D MRDSA between November 9, 1999, and June 11, 2001 were prospectively evaluated. Informed consent was obtained from all participants after the nature of the procedure had been thoroughly explained. Eleven patients underwent two 2D MRDSA examinations, which were treated as separate cases in the database. Thus, a total of 78 2D MRDSA examinations were included in the analysis. Patent AVM was present in 55 cases, whereas the remaining 23 cases involved AVMs that had been obliterated following gamma-knife radiosurgery, as confirmed on the basis of gold standard IADSA diagnostics. The study population included 41 male and 37 female patients with a mean age of 36.3 years (range, 10 to 67 years). The examinations included 33 pre- and 45 post-gamma-knife radiosurgery cases. All pre-gamma-knife studies were obtained within 4 days prior to the therapy,

while the post-gamma-knife examinations were performed at least 5 months after the treatment (5 to 117 months; mean, 39.0 months). Routine pre- and post-contrast MR imaging including T2-weighted imaging (T2WI) and 2D MRDSA was conducted with a 1.5-T MR unit (Signa Horizon, General Electric, Milwaukee, Wis.). In 53 of 78 cases, IADSA was performed within 2 days of 2D MRDSA, and 32 of these 53 IADSA studies were performed within 5 days prior to gamma-knife radiosurgery. Informed consent was obtained from each patient or the patient's guardian prior to MRDSA and IADSA.

Two-dimensional magnetic resonance digital subtraction angiography (MRDSA) sequence

The 2D thick-slice, ultra-fast continuous scan with a bolus injection of contrast material was performed by fast spoiled gradient-echo sequence (TR/TE, 5.4/1.5 ms;

flip angle, 60–90°; FOV, 24 × 24 cm; matrix size, 512 × 192; bandwidth, 62.5 kHz; slice thickness, 70–80 mm). Images were obtained every 1.05 second after initiation of bolus injection of 20 mL gadolinium chelates (generally at 8 mL/sec, although a slower rate was used when placement of a large needle was difficult), followed by 20 mL of saline, for a duration of up to 60 seconds on primarily sagittal planes covering a hemisphere. The final image prior to contrast arrival (mask image, predominantly around the tenth frame) was selected on the display and subtracted from later images. Subtraction images (simple subtraction) were generated with commercially available software (Advantage Windows, General Electric, Milwaukee, Wis.). Approximately 30 subtracted images were reconstructed within 1 min. Twenty of 60 subtracted images were inverted by intensity and filmed for evaluation.

Image analysis

Qualitative image analysis was independently conducted by two observers who were blinded to the IADSA results during the initial reading of the 2D MRDSA images. Each observer evaluated anatomic depiction of key components of the AVM, including nidus flow voids on T2WI, feeding vessels, draining vessels, nidi, and early venous filling on 2D MRDSA. When applicable, the 2D MRDSA images were then compared with corresponding IADSA studies performed within about two days. All items were rated on a three-point scale, with 1 = absent, 2 = equivocal, and 3 = present. In cases of inter-observer disagreement, final decisions were reached by consensus. Cohen's kappa values were calculated to establish inter-observer variance at the initial evaluation.

6-3. 【Results】

No complications were reported during 2D MRDSA procedures. At the initial assessment of nidus flow voids on T2WI and feeding vessels, nidi, draining vessels, and early venous filling on 2D MRDSA, the observer ratings were in agreement in 68 (87%), 69 (88%), 74 (95%), 75 (96%), and 75 (96%) cases, respectively; Cohen's kappa values (κ) were 0.77, 0.80, 0.90, 0.93, and 0.92, respectively. In the 55 studies representing patent AVM, the mean visualization ratings for nidus flow voids, feeding vessels, nidi, draining vessels, and early venous filling on MR imaging were 2.8 (κ = 0.68), 2.4 (κ = 0.69), 2.6 (κ = 0.89), 2.8 (κ = 0.80), and 2.8 (κ = 0.76), respectively. On occasion, when large feeding vessels were visible on 2D MRDSA, the feeding and draining vessels could be distinguished in separate frames of the 2D MRDSA (**Figs. 2-1, 2-2**) examinations. In instances involving AVMs accompanied by abnormal intensities of hemosiderin or some other substances due to hematoma, the subtraction technique allowed easy recognition of nidi and draining vessels by suppression of the

signal from the hematoma. The results of the 2D MRDSA and T2WI evaluations and the comparison of T2WI and 2D MRDSA findings are shown in Table 2-1 to 2-3. The sensitivity, specificity, positive predictive value, and negative predictive value for detection of AVM by 2D MRDSA were 87%, 100%, 100%, and 78%, respectively (**Table 2-1**), while the sensitivity, specificity, positive predictive value, and negative predictive value for nidus flow voids on T2WI were 80%, 91%, 96%, and 66%, respectively (**Table 2-2**). Nidus flow voids were equivocal or absent on T2WI in 4 of 78 cases, but early venous filling was clearly depicted on 2D MRDSA (**Tables 2-3**).

In 22 of 45 post-obliteration follow-up studies, IADSA was performed within 2 days of the 2D MRDSA examination. Residual AVM was visible on IADSA in 13 of these 22 cases; in 4 of these cases, 2D MRDSA could not clearly demonstrate early venous filling, while in 9 instances, it correctly predicted incomplete obliteration.

6-4. 【Discussion】

Gamma-knife radiosurgery is an effective form of treatment for about 70% of patients harboring AVMs (11). Residual AVM carries a risk of hemorrhage, and follow-up studies are required to confirm complete obliteration following radiosurgery. Conventional catheter angiography (IADSA), which is regarded as the gold standard for diagnosis of AVM, also carries some risk (5, 24). MRI and MRA can be used to estimate the size of the nidus and to detect radiation-induced changes after radiosurgery (22). During the typical follow-up after gamma-knife radiosurgery (11), in instances where an obvious AVM nidus is visible on conventional MRI performed at 4- to 6-month intervals for 2 years, IADSA is recommended. Where evidence of AVM remains on IADSA at 2 years, a 3-year follow-up angiogram is recommended. According to this schedule, a patient presenting with AVM will undergo IADSA about 3 times on average, including the initial diagnostic or planning study prior to radiosurgery. Since the location of the AVM has been shown on the preoperative

IADSA evaluations, it is likely that the lesion can be adequately chased by my 2D MRDSA technique at the follow-up evaluation, and the availability of this new method may allow for the number of more invasive IADSA procedures to be limited to 1 or 2 examinations.

Non-contrast TOF MRA is currently the established method for non-invasive evaluation of cerebral arteries (41, 76), and the use of dynamic CE MRA techniques for the assessment of the aorta and its branches (27, 51, 52) as well as in the assessment of the neck, pelvis, and extremities (55, 59, 60, 77, 78, 79) has rapidly increased. Non-contrast 3D TOF MRA is not suited for visualization of slow flow, as flow-related enhancement (i.e., the inflow effect) may not persist in the venous system or in the distal portion of the slow-flow vessels (31, 76). The use of MR contrast agents may allow a greater sensitivity for the detection of slow flow in vessels because they produce remarkable shortening of intravascular T1 relaxation times (52). Thus, in

comparison with non-contrast flow-dependent MRA, 3D CE MRA is useful for the assessment of slow flow, especially within the distal portion of severely stenotic or occluded lesions (55, 60, 77). Abnormalities indicating feeding vessels are the main finding indicative of AVMs by flow-dependent MRA, but for some small lesions, early venous filling detected by IADSA may be the only clue, meaning that flow-dependent MRA may be insufficient in terms of locating small AVMs with narrow feeding vessels. To address this, several authors have proposed contrast-enhanced time-resolved MRA or MRDSA (3, 18, 21, 26, 33, 52, 68, 80) for improved temporal resolution of MRA.

At present, the majority of CE MRA studies are performed with 3D acquisition. Advances in MR technology have allowed 3D CE MRA with high temporal resolution, and state-of-the-art 3D MRDSA techniques, such as 3D TRICKS (33), can provide temporal resolution of 2 to 6 sec and enable the separation of arterial and venous phases in most portions, although, because of the rapidity of the intracranial circulation,

it has remained difficult to separate arterial and venous phases in the brain; the reduced scan times (increased frame rates) associated with 2D acquisition techniques for CE MRA may be useful in these cases, as has been reported (1, 3, 14, 21, 26, 35, 68, 71, 80). In fact, the 2D technique in lieu of a 3D method readily reduces the scan time to less than 1 sec. In addition, the 2D procedure permits acquisition of intracranial hemodynamic information similar to that obtained with IADSA, including the separation of the arterial and venous phases. The technique of contrast-enhanced 2D thick-slice MRDSA with high temporal resolution presented here was able to demonstrate intracranial hemodynamics in a fashion similar to that shown by conventional IADSA, and when sufficiently large feeding vessels were visible on 2D MRDSA, feeding vessels, nidi, and draining vessels could also occasionally be distinguished on different frames of 2D MRDSA (**Fig. 2-1**). The images produced by 2D MRDSA were very similar to those of conventional IADSA, and the cine mode

display on a workstation allowed ready visualization of intracranial hemodynamics without the cumbersome process of comparison of pre- and numerous post-contrast images. The method of image interpretation for 2D MRDSA is also similar to that of conventional IADSA, and thus should be a very familiar method for neuroradiologists. Because it is still the gold standard, IADSA is necessary at some point during follow-up after radiosurgery, and an additional advantage of 2D MRDSA is that it is easy compared with the conventional IADSA studies by a similar display.

Although nidus flow void has been regarded as a relatively reliable lead to AVM, its sensitivity is not high in comparison to its nearly perfect specificity (50). When the continuity of an absence of signal intensity can be confirmed, it is a definitive sign of the presence of flow void. However, because AVMs are often accompanied by hemorrhage, consequent hemosiderin depositions around nidi lead to confused interpretation. Moreover, thrombosed vessels may show hypointensity that mimics

flow void. Furthermore, the appearance of the flow void often varies due to distinctions associated with machine type, slice thickness, echo trains, and other setup factors. Indeed, in the present results, agreement of two observers in terms of rating of nidus flow voids was also low; however, on 2D MRDSA, despite the presence of hematoma, the nidi and draining vessels were readily recognized because of the suppression of signal from the hematoma resulting from the subtraction technique. Theoretically, demonstration of early venous filling on 2D MRDSA is thought to be superior to the finding of nidus flow void on T2WI in the assessment of AVM. I encountered several cases in which residual AVMs were clearly recognized with early venous filling on 2D MRDSA while the nidus flow voids were equivocal or absent on T2WI (**Table 2-3**), although it was also true that within the same patient population, there were several instances involving the detection of nidus flow voids in the absence of early venous filling. In the case of especially small AVMs, it may be difficult to

discern early venous filling on 2D MRDSA as a consequence of poor spatial resolution.

Among various MR and CT angiographic (CTA) techniques, contrast-enhanced 2D MRA is considered the most appropriate method with respect to visualization of cerebral hemodynamics with high temporal resolution (3, 21, 26, 68, 80). Other techniques such as TOF MRA, PC MRA, first-pass CE MRA, and 3D CTA exhibit high spatial resolution and can provide 3D information as well and although temporal resolution is usually low with these techniques and the detection of early venous filling is relatively poor, the delineation of anatomic structures is excellent. Source images of CE MRA or 3D CTA, or contrast-enhanced spoiled gradient-echo images, can depict the nidus of the AVM itself (2, 22), and these images are useful for the planning of stereotactic radiosurgery (2, 22). A drawback of the high spatial resolution of these images is the potential for over-detection of enhanced structures such as post-surgical

changes, radiation-induced changes, and enhanced resolving hematomas, which may be misinterpreted as nidi of AVMs and may make judgment as to whether complete removal or obliteration has been attained after surgical, interventional, or radiation treatments difficult. The presence of residual AVM must ultimately be confirmed by its patency in the end, and for this, my 2D MRDSA technique can furnish additional information regarding hemodynamics with relatively little cost and risk. Furthermore, as opposed to the substantially increased evaluation times resulting from the large number of high spatial resolution images, 2D MRDSA results are displayed in similar fashion to IADSA images and are readily interpreted. Obtaining 2D MRDSA images with contrast requires only a short period of time with minimal post-processing. IADSA provides more precise hemodynamic information, but, as noted, it is invasive and is also accompanied by greater expense, and increased time and labor requirement, again stressing the potential advantage of 2D MRDSA in terms of the reduced need for

repeated IADSA examinations.

There are several limitations to 2D MRDSA. First, in cases of exceptionally small AVMs, location of lesions may be vague if site information is not disclosed beforehand. In follow-up studies, this disadvantage can be avoided by referring to previous IADSA images, ensuring that imaging with 2D MRDSA when only traces of AVM remain following obliteration treatment is not necessarily useless. Secondly, small vessels may be obscure, probably due to the partial volume effect. The mean ratings for visualization feeding vessels were low, as this vasculature is generally smaller than nidi and draining vessels. Early venous filling may be the sole diagnostic indicator in cases of small AVMs or post-operative, embolized, or irradiated AVMs with slow flow. Thus, visualization of feeding vessels is not necessarily required for follow-up studies. Third, overlap of vessels cannot be eliminated by alteration of view angles, as may be possible with 3D imaging; this is one of the results of the trade-off between high

temporal resolution of 2D imaging and high spatial resolution of 3D imaging. The temporal resolution of 2D MRDSA does not surpass that of IADSA, but it is adequate for identification of the flow of contrast material through each component of the AVM (**Figure 2-1, 2-2**), and 2D MRDSA can, therefore predict the existence of residual AVM and demonstrate hemodynamic changes following treatments such as gamma-knife radiosurgery. Since frequent or periodic post-treatment examinations are required for patients with AVM, it is useful to have reliable imaging techniques, such as 2D MRDSA, that are less invasive and carry a lower known risk of radiation exposure, than the conventional IADSA techniques.

6-5.【Conclusion】

Two-dimensional thick-slice contrast-enhanced MR digital subtraction angiography (2D MRDSA) exhibits sufficient temporal resolution to evaluate intracranial hemodynamics in patients presenting with small- to medium-sized AVMs. The temporal resolution is similar to that of conventional catheter angiography (IADSA). My results indicate that 2D MRDSA has the potential to serve as a less invasive dynamic angiographic method for follow-up evaluations in patients who have been treated for intracranial AVMs diagnosed by IADSA.

7. Part 3: Magnetic Resonance Digital Subtraction Angiography Using Array Spatial Sensitivity Encoding Techniques in Assessment of Intracranial Hemodynamics

7-1. 【Introduction】

Two-dimensional (2D) thick-slice contrast-enhanced magnetic resonance digital subtraction angiography (MRDSA) has been shown to be a suitable approach for assessment of cerebral hemodynamics; in specific clinical situations, it may be an alternative to conventional catheter angiography (3, 21, 68, 80). In combination with a T1-shortening contrast agent and a digital subtraction technique, 2D thick-slice fast spoiled gradient-echo sequence provides 2D angiograms characterized by high temporal and spatial resolution.

High temporal resolution imaging is essential in the diagnosis of some intracranial lesions, such as arteriovenous malformations and fistulas (AVM/F). Early venous filling on conventional catheter angiography may be the only diagnostic clue with respect to detection of small hemorrhagic AVMs and postoperative, embolized, or

irradiated AVMs. Due to marked shortening of intravascular T1 relaxation times, contrast-enhanced MRA is more sensitive to slow flow than is non-contrast imaging (31, 51, 76). The acquisition time (increase frame rate) of contrast-enhanced MRA images is readily reduced by use of the 2D technique, and hemodynamic information similar to that obtained with conventional catheter angiography (IADSA) can be acquired, including separation of arterial and venous phases (3, 21, 68, 80).

Parallel image-encoding techniques (**Appendix 2**) such as array spatial sensitivity encoding (ASSET, General Electric, Milwaukee, Wis.) and sensitivity encoding (SENSE, Philips Medical Systems, Best, Netherlands), facilitate reduced acquisition times in most MRI sequences via exploitation of information related to the distinct spatial sensitivities of coil array elements (54, 71, 74, 75). This process is affected when coil sensitivities are used as a means of signal encoding complementary to gradient switching, resulting in scan time reductions secondary to reduction in the

number of required phase encoding steps. Few studies on the use of the parallel imaging approach to reduce the acquisition time of contrast-enhanced MRA are available (75), and to my knowledge, this technique has not been applied to the evaluation of intracranial hemodynamics.

In this investigation, I propose combination of a 2D fast spoiled gradient-echo (FSPGR) sequence with ASSET to generate 2D MRDSA images characterized by improved temporal resolution. A two-fold ASSET reduction factor was utilized and images produced by 2D MRDSA using ASSET were compared with those generated conventional 2D MRDSA performed during the same examination, when available.

7-2. 【Materials and Methods】

Patients

A total of 28 patients who were referred to my institution for brain hemodynamic MR examinations from March 16 to May 28, 2001 underwent prospective examination by 2D MRDSA with ASSET. The study group included 15 men and 13 women with a mean age of 43.1 years (range, 19 to 84 years). There were 12 patients with AVM (8 with AVM proven by conventional IADSA, and 4 who had undergone gamma-knife radiosurgery), 11 with brain tumors, 2 cases of infarction, a single case of AVF, and one patient with angiitis. Among the brain tumors, there were 4 meningiomas, 3 metastatic lesions, 1 glioma, 1 hemangioblastoma, 1 hemangioma, and a single hamartoma.

Routine pre- and post-contrast MRI and 2D MRDSA were conducted with a 1.5-T MR unit (Signa Horizon Echo Speed, General Electric, Milwaukee, Wis.).

Conventional 2D MRDSA (in the absence of ASSET) was also performed in the same

examination in 10 of 28 patients for purposes of comparison. Informed consent was obtained from each patient or the patient's guardian prior to MRDSA and IADSA.

Array spatial sensitivity encoding techniques (ASSET)

Array spatial sensitivity encoding is a fast parallel-encoding imaging technique employing multiple receiver coils that exploits information related to the distinct spatial sensitivities of the coils (54, 71, 74, 75), which allows for reduction of the number of gradient phase encoding steps in order to speed image acquisition. The reduction of the number of phase-encoding steps with respect to full Fourier encoding is denoted by the ASSET reduction factor R. This reduction in phase encoding steps results in immediate, significant reduction of acquisition time.

A flexible wraparound coil array (torso coil) consisting of four elliptical elements (20 × 30 cm) was employed to achieve a two-fold ASSET reduction (R = 2) along the

left-right phase encoding direction. Sensitivity-based image reconstruction has important implications for the signal-to-noise ratio (SNR) of the resulting data, and ASSET theory predicts that, unlike standard Fourier MRI, the noise level of volume data in ASSET images is not homogeneous. Rather, the noise level undergoes enhancement in regions where sensitivity relations are not optimal, and this effect is described by the local geometrical SNR factor g, which depends on the imaging setup.

In the present implementation, the fast Fourier transform step was performed on the MR scanner and ASSET reconstruction was executed off-line using MATLAB 6 (Release 12, Cybernet Systems Co., Ltd, Tokyo, Japan) on a Sun Ultra 5 workstation (Sun Microsystems, Palo Alto, USA).

Two-dimensional magnetic resonance digital subtraction angiography (MRDSA) sequence

Two-dimensional thick-slice, ultra-fast continuous scan with a bolus injection of contrast material was performed by FSPGR sequence and an array of receiver coils was used for ASSET. The imaging parameters of 2D MRDSA with ASSET were as follows: TR/TE, 5.4/1.5–1.6 ms; flip angle, 60°; FOV, 24 × 24 cm; matrix size, 256 × 256; (single) slice thickness, 50 mm (25 patients), or TR/TE 5.6–7.6 /1.3–1.6 ms and slice thickness, 70 mm (3 patients: one with glioma, one with hemangioma, and one with infarction). The imaging parameters for conventional 2D MRDSA using head coils (10 patients) were as follows: TR/TE, 5.4–5.5 /1.5 ms; flip angle, 60°; FOV, 24 × 24 cm; matrix size, 256 × 256; slice thickness, 50 mm. Images were obtained after the initiation of a bolus injection of 20 mL gadolinium chelates at 8 mL/sec, followed by 25 mL of saline flush, for a duration of up to 40 sec on a sagittal plane covering the disordered hemisphere determined by conventional MRI. ASSET reconstruction was performed off-line on the aforementioned workstation. The last image prior to contrast

arrival was selected on the display as a mask image and subtracted from later images. Subtraction images (simple subtraction) were generated with commercially available software (Advantage Windows, General Electric, Milwaukee, Wis.). Twelve to twenty of all subtracted images were inverted by intensity and filmed for evaluation.

Image analysis

Two observers independently performed qualitative image analysis. In cases of interobserver disagreement, final decisions were reached by consensus. Visualization of normal cranial vessels observed on 2D MRDSA using ASSET and on conventional 2D MRDSA was rated independently in blind fashion as follows: 1 = not seen (including outside of FOV); 2 = seen but deteriorated; 3 = clearly seen. Observers evaluated the anatomic depictions of the distal internal carotid artery (ICA), the ophthalmic artery, the A1 and A2 segments of the anterior cerebral artery (ACA), the

A3 and A4 segments of the ACA, the M1 and M2 segments of the middle cerebral artery (MCA), the M3 and M4 segments of the MCA, the distal vertebral artery (VA), the basilar artery (BA), the posterior cerebral artery (PCA), the superior sagittal sinus (SSS), the straight sinus, the deep cerebral veins, the transverse/sigmoid sinus, and the jugular vein. In instances where the A1 or M1 segment overlapped with the distal ICA, the A2 or M2 segment was estimated exclusively. In 10 of 28 cases, 2D MRDSA using ASSET was paired and compared with the corresponding sites on conventional 2D MRDSA that had been performed in the same examination.

In patients with AVMs, the draining vessels of the AVMs and early venous filling were evaluated on the 3-point scale described. In patients with brain tumors, tumor stains on 2D MRDSA using ASSET were compared with those on conventional 2D MRDSA.

Cohen's kappa values were calculated in order to ascertain interobserver variance of

evaluation at the initial review and Spearman rank correlation was utilized to examine the associations between the visualization ratings for 2D MRDSA with ASSET and those for conventional 2D MRDSA.

7-3. 【Results】

ASSET acquisition and reconstruction were performed successfully in all but one examination during which sufficient data could not be obtained due to the patient's head movement during dynamic scanning.

An ASSET reduction factor of two was demonstrated. ASSET facilitated improvement of the temporal resolution (frame rate) of a 256 × 256 matrix, from 1.45 second to 0.77 second per image, without loss of spatial resolution, The reconstruction time of 2D MRDSA images using ASSET with 5-cm slice thickness was approximately 40 minutes and was higher with a 7-cm slice thickness.

Table 3-1 summarizes the mean ratings for visualization of normal cranial vessels in 24 patients (data of one patient were excluded as noted above) who underwent 2D MRDSA using ASSET with 5-cm slice thickness on a sagittal plane. The data of 3 studies using 7-cm slice thickness were substantially poorer and were omitted from the table.

Table 3-2 summarizes the correlation between vascular visualization by 2D MRDSA using ASSET and that of conventional 2D MRDSA. The 2D MRDSA with ASSET provided somewhat poorer visualization in comparison with conventional 2D MRDSA because of lower ratings for visibility of small vascular structures.

Figures 3-1 and **3-2** show a comparison of image quality obtained with the two techniques. In all 10 patients who underwent comparison studies, the 2D MRDSA images with and without ASSET were nearly identical in terms of contrast. However, on the 2D MRDSA images with ASSET, the vascular edges were less distinct and the visibility of small vessel branches was slightly diminished.

Nearly all draining veins in patients with patent AVM (8/8) were clearly detected by 2D MRDSA imaging with ASSET, while some draining vessels were overlooked on conventional 2D MRDSA. Decreased temporal resolution creates ambiguities with respect to discrimination between early venous filling and normal venous return

because these events appear on the same image, and **Figure 3-1** demonstrates that draining vessels were more readily perceptible on 2D MRDSA using ASSET than on conventional 2D MRDSA. In 4 patients who had undergone gamma-knife radiosurgery of AVM, 2D MRDSA using ASSET correctly predicted that there was no residual lesion, and this finding was confirmed by conventional IADSA performed at a later date.

Tumor stains were present in all 4 cases of meningioma, and both imaging methods detected a first-pass stain in the patient with hemangioblastoma. A stain was also evident in one hemangioma involving the right cavernous sinus. Stains were not obvious in the remaining 5 brain tumors (11 cases total) with either method.

7-4. 【Discussion】

Conventional catheter angiography (IADSA) has been the gold standard for assessment of intracranial hemodynamics, but it is associated with a number of risks (5, 24). Non-contrast TOF-MRA and PC-MRA are established methods for non-invasive evaluation of cerebral blood vessels (41, 76) but these methods provide only static images of vascular structure and cannot provide hemodynamic information. Dynamic contrast enhanced (CE) MRA is available for vessels of the trunk and extremities (27, 51, 52, 55, 59, 60, 77, 78, 79), but the techniques are not generally applicable to the rapid intracranial circulation because separation of arterial and venous phases cannot be readily accomplished.

A number of attempts to accelerate CE MRA acquisition using conventional methods have been reported, but most are associated with unacceptable losses in spatial resolution. However, the usefulness of 2D acquisition techniques for reduced acquisition times (increase frame rate) of CE MRA in comparison to the 3D modality

has been reported (3, 80), and in these reports, it is shown that 2D MRDSA is able to differentiate the arterial and venous phases of the rapid cerebral circulation. ASSET is a promising new technique that also shortens acquisition time by reducing the number of gradient phase encoding steps by substituting the information acquired by arrays of receiver coils with known sensitivities. Theoretically, the ASSET technique can be applied to all sequences. Thus, the combination of 2D MRDSA and ASSET should provide further improvement in temporal resolution without compromising spatial resolution.

In the present study, large cerebral arteries including ICA, proximal ACA, VA, and BA were clearly depicted. Smaller arterial branches tended to be less visible in comparison with large arteries. Middle portions of MCA (M2 and M3) tended to be out of FOV due to narrow slice thickness (5 cm); consequently, ratings for visualization of distal MCA were lower than those for visualization of proximal MCA. Visualization of

venous sinuses and tributaries tended to be better than that of most other arterial structures. These tendencies were compatible with previous reports as to conventional 2D MRDSA (3, 80). However, 2D MRDSA using ASSET displayed slightly reduced vascular visualization in comparison with conventional 2D MRDSA due to poorer ratings for small vascular structures (**Table 3-2**). When conventional 2D MRDSA scans were acquired for comparison with ASSET studies, there was residual contrast agent from the preceding ASSET scan visible in the wide blood vessels and subcutaneous tissues of pre-subtraction images that became less conspicuous following the digital subtraction procedure. Generally, the SNR decreases due to the ASSET reduction factor R and the geometrical SNR factor g. However, as a consequence of the high baseline SNR of CE MRA, this SNR reduction did not have a perceptible impact on the diagnostic value of the resulting subtraction images obtained in this study. The most noticeable difference between the two methods was the existence of residual

fold-over artifacts on the images acquired with ASSET.

On the other hand, despite these disadvantages, the higher temporal resolution of the ASSET images resulted in superior and more precise depiction of intracranial hemodynamics on the first pass of the contrast agent, including visibility of a pure capillary phase between the arterial and venous phases and of a pure venous phase prior to arterial recirculation. Although the temporal resolution did not surpass that of traditional IADSA, it was adequate with respect to identification of the flow of contrast material through each portion of the intracranial vasculature.

It is particularly desirable to avoid multiple invasive arterial catheterization procedures in children, and 2D MRDSA may allow this. Moreover, as children possess faster circulation times in comparison with adults, the improved temporal resolution associated with 2D MRDSA using ASSET may be extremely useful, as it provides even more precise hemodynamic information than does conventional 2D MRDSA. The

availability of cine mode displays on workstations facilitates examination of intracranial hemodynamics without troublesome comparisons involving numerous pre- and post-contrast images, and the similarity of images produced by 2D MRDSA to those produced by conventional IADSA is helpful to the examining neuroradiologists.

A basic requirement for obtaining artifact-free ASSET reconstruction is an identical coil configuration for the reference and the contrast-enhanced scans. Since the head can be adequately fixed during the examination, the ASSET technique is suited for the head scan. At present, only torso coil is available for ASSET processing. Nevertheless, a rigid frame for the head scan might be convenient for better examination efficiency.

In theory, the ASSET technique, in addition to reducing scan time in 2D MRDSA, can be used to improve spatial resolution or SNR. For example, doubling the repetition time under ASSET, i.e., substantially maintaining an acquisition time identical to that of conventional 2D MRDSA, may result in improved SNR and sharpened image

quality due to T1 relaxation. On the other hand, 2D MRDSA offers the possibility of controlling the signal level via dosage and injection rate of the contrast agent. For instance, at a constant scan time, a higher SNR can be attained by injection of elevated total doses of contrast agent at a higher rate. However, the signal gain achievable with high concentrations of contrast agent concentrations is limited by the concurrent loss due to increased T2* decay (64).

My novel method of 2D MRDSA using ASSET had several limitations. First, visualization of vascular structures was relatively vague in comparison to conventional 2D MRDSA. Blurring at vascular edges may be attributable to insufficient sensitivity compensation or decreased sampling data of high frequency components divided by each receiver coil, impaired SNR, or other factors. Additionally, smaller vessels tend to be further obscured as a consequence of the partial volume effect. Increased slice thickness itself may adversely influence the ASSET procedure, e.g., via deterioration

of the geometrical factor g.

In contrast to conventional image reconstruction, ASSET processing includes intensity correction, i.e., compensation for non-homogeneous coil sensitivity. While this does not affect SNR, it does result in non-homogeneous noise scaling. The two methods differ in the behavior of image SNR and as a result, direct comparison cannot be achieved due to the use of different coils in the two methods. Generally, geometry-related noise enhancement, as specific for ASSET reconstruction, is described by the geometrical SNR factor g; moreover, at two-fold reduction in the left-right direction, the applied coil arrangement warrants geometrical factors approaching the optimum value of 1.0. This phenomenon occurs for each pair of aliased pixels because the sensitivity relations between the four coils are clearly distinct.

Secondly, at the present time, the aliasing artifact remains slight, which may be due

to inadequate sensitivity compensation. Generally, this artifact can be distinguished easily from intracranial structures when it exhibits a typical shape at typical locations. However, it is occasionally difficult to observe the site overlapped by this artifact; this was demonstrated in the present study when we encountered a single patient displaying a wrap-around stain of nasal mucosa that mimicked the nidus of a parietal AVM.

Third, approximately 40 minutes were required to generate one series of 256 × 256 matrix images, and additional time was necessary to generate 512 × 192 matrix images, which was attributable to off-line reconstruction. Nevertheless, provisions for on-line reconstruction are available, which can result in completion of post-processing within several minutes.

7-5.【Conclusion】

The usefulness of ASSET for improving the temporal resolution of 2D MRDSA was examined. ASSET is able to evaluate each slice of a 2D MRDSA sequence in sub-second order, permitting satisfactory evaluation of patients with AVM, and I have concluded that 2D MRDSA with ASSET possesses an important advantage in terms of its potential to serve as an alternative to more invasive conventional IADSA procedures.

8. Part 4: Clinical Application of 3-Tesla Time-Resolved, Contrast-Enhanced, Three-Dimensional Magnetic Resonance Angiography to Arteriovenous Malformations

8-1. 【Introduction】

The diagnosis of cerebral AVM requires delineation of its components: location, size, nidus morphology, feeding arteries, and draining veins. In the pretreatment evaluation, conventional catheter angiography (IADSA) is regarded as the most suitable tool because of its high spatial and temporal resolution. Its clinical complication rate of <1% (12) is considered acceptable against its benefit of proving key information on small feeding arteries and draining veins that is required by clinicians for determining the best management options for the affected patients (i.e., neurosurgical intervention, endovascular embolization, or stereotactic irradiation).

In screening and follow-up examinations, however, less invasive diagnostic tools with less or no radiation exposure are desirable. Thus, the use of contrast-enhanced MR angiography (MRA) with high spatial resolution has become an accepted

alternative to conventional IADSA for the screening and post-treatment assessment of AVM (16, 32).

Time-resolved imaging of contrast kinetics (TRICKS, **Appendix 3**) is a new method of time-resolved 3D MR digital subtraction angiography (DSA) (33) that can achieve adequate temporal and spatial resolution for evaluation of AVMs (10, 17, 19, 42, 75), especially with 3-T imaging (7, 8, 58). In this study, I investigated the accuracy of 3-T TRICKS vs. conventional IADSA in the assessment of AVM.

8-2. 【Materials and Methods】

Patients

I searched my hospital's imaging records from the period between November 2006 and November 2007, and recruited 31 patients (14 men and 17 women; mean age, 38.3 years; range, 16–74 years) who were known to have or to have had AVMs (**Table 4-1**). All patients underwent conventional catheter angiography and TRICKS with the 3-T system with an interval of <1 month between modalities. All patients had an adequate glomerular filtration rate (>30 mL/min/1.73 m^2) and were referred for MR imaging according to the accepted protocol for the clinical evaluation of AVM at my institution. Informed consent was obtained from each patient or the patient's guardian prior to MRDSA and IADSA.

Twenty-three AVMs were located in the supratentorial circulation (2 frontal, 7 parietal, 6 temporal, 5 occipital, 1 basal ganglia/thalamus, and 2 in the corpus callosum) and 4 were in the infratentorial circulation (1 pons, 1 cerebellum, and 2 in

the cerebellopontine angle). In the remaining 4 cases, the AVMs were angiographically obliterated after radiosurgery.

Magnetic resonance imaging

The MRI examinations were performed with a 3-T superconducting system (Signa 3.0 T HDx System, GE Healthcare). Time-resolved imaging of contrast kinetics (TRICKS) was performed in combination with conventional MRI sequences. The images were obtained in the sagittal plane, including imaging of the internal carotid artery on the lesion side in all cases. The imaging parameters for TRICKS were as follows: TR, 4.3 msec; TE, 1.5 msec; flip angle, 20°; FOV, 240 × 190 mm; acquisition matrix, 384 × 256; section thickness, 4.0 mm (resolution doubled using zero-fill interpolation processing) to obtain 6.4-cm volume coverage, 83.3-kHz bandwidth, and an excitation value of 0.5. Parallel imaging with a reduction factor of 2 was applied. The TRICKS

reconstruction generated 48 time-resolved phases with a frame rate of 0.8 seconds per volume. About 15 mL of gadoteridol (Prohance, Bracco) or gadodiamide (Omniscan, Nycomed) was injected at 4 to 10 mL/second with a power injector (Spectris Solaris EP). The first volume was subtracted from subsequent volumes to eliminate background nonvascular signal intensity and then the MIP was reconstructed.

Conventional catheter angiography (IADSA)

IADSA was performed with a 4 or 5 Fr catheter via the femoral artery and a filming rate of 2 to 3 images/second, a 1024 × 1024 matrix size, and a 20-cm FOV. Angiography included selective injection of the internal carotid, common carotid, or vertebral arteries in the frontal and sagittal views and additional views as necessary. For each projection, a 6 to 18 mL bolus of iodinated contrast material, iopamidol (Iopamiron, Japan Schering) or ioversol (Optiray, Yamanoushi Pharmaceutical), was

injected at 2 to 6 mL/second using a power injector.

Image interpretation

Two neuroradiologists, both blinded to the results of either study, independently reviewed the TRICKS results using source and maximum intensity projection (MIP) images. For the initial evaluation, observers checked for a patent nidus. Next, in cases of patent nidi, the characteristics were evaluated according to the Spetzler-Martin classification (63). Nidi were classified into 1 of 3 groups according to size: small (<3 cm), medium (3 to 6 cm), and large (>6 cm). Venous drainage was categorized as superficial only or including the deep venous system, and the location was categorized as being in an eloquent or noneloquent area. The venous drainage was defined as superficial if the veins drained into the cortical venous system and as deep if the veins drained into the great vein of Galen, the straight sinus, or the cavernous sinus. After

evaluation of each factor, the grade was calculated according to the scoring system (63). Early venous filling was evaluated in addition to the Spetzler-Martin classification in cases of patent nidi.

The IADSA examination results were reviewed by 2 other neuroradiologists as reference images. Each AVM shown on the conventional catheter angiography films was analyzed in a same manner as the TRICKS images.

Statistical analysis

All statistical studies were performed with commercially available software (JMP 6, SAS Institute). Kappa values were calculated for Spetzler-Martin grade agreement of TRICKS between both observers, and correlation with the results of the IADSA evaluations. The Wilcoxon signed-rank test was used to analyze interobserver variability on nidus and early venous filling detection. Sensitivity and specificity were

calculated to assess the diagnostic accuracy of TRICKS compared with that of IADSA in terms of detection of nidi and early venous filling. Kappa values of up to 0.4 indicated a positive agreement but poor correlation, 0.41 to 0.6 reflected moderate agreements, 0.61 to 0.8 indicated good agreement, and values of 0.81 to 1 indicated an excellent agreement or correlation. For Wilcoxon signed-rank tests, probability values (p) <0.05 were regarded as significant.

8-3. 【Results】

No complications were reported during the MR or IADSA procedures. We successfully obtained continuous serial hemodynamic images in all 31 cases. Of the 31 patients, 4 had AVMs that were angiographically obliterated after treatment. Embolization had previously been performed for 2 AVMs and radiosurgery for 4; there were 2 cases with residual hematomas detected by TRICKS.

Interobserver agreement

There was complete agreement between 2 observers in nidus detection ($p > 0.05$). With regard to the detection of early venous filling, there was disagreement in only 1 case ($p > 0.05$). Interobserver agreement was good for Spetzler-Martin grade ($\kappa = 0.61$): there were discrepancies between the 2 observers regarding nidus size in 3 cases, location in 3, and visualization of venous drainage in 3 cases. In the cases with interobserver disagreement, an additional reading by both examiners was performed to reach a

consensus.

Nidi and detection of early venous filling

All 4 cases of occluded AVM were correctly diagnosed on TRICKS (specificity of nidus detection, 100%). In addition, one very small nidus (<10 mm) in the right occipital lobe without early venous filling was also correctly evaluated on TRICKS (specificity of early venous filling detection, 100%). Sensitivity was 96% for both nidus detection (26/27) and detection of early venous filling (25/26) (**Figs. 4-1, 4-2**). In one case, the nidus was not obvious, but a small dilated draining vein in the left cerebellopontine angle with early venous filling was seen on IADSA (but not on TRICKS), and I regarded this as a finding consistent with a very small patent AVM, which was not detected on TRICKS.

Spetzler-Martin classification

Two cases were excluded from assessment with the Spetzler-Martin classification. In the first case, mentioned in the previous section, the nidus could not be visualized clearly on IADSA. In the other case, the nidus was seen at the temporal tip, and in the FOV to focus on the location of the nidus, the great vein of Galen was excluded.

Nidus size and location

Eleven nidi were classified as small, 12 as medium, and 2 as large on IADSA. The results of TRICKS were matched to those of conventional catheter angiography in 24 cases (**Table 4-2**). It was difficult to measure the exact size of the nidus in the sagittal plane on source images in 1 case because a dilated draining vein lay over the nidus. In 1 case, the nidus was 32 mm in diameter with a dilated draining vein overlaid in the sagittal view, which made it difficult to measure the exact size of the nidus in the

sagittal plane even on source images. Both observers regarded this nidus as small (<3 cm).

IADSA showed 12 nidi located in eloquent areas and 13 in noneloquent areas, and there was complete agreement between IADSA and TRICKS for determination of nidus location.

Venous drainage

Of the 25 AVMs, 14 had deep venous drainage demonstrated by IADSA, and 11 showed exclusively superficial drainage. TRICKS diagnosed the drainage route correctly in 24/25 cases (**Table 4-2**). In 1 case, TRICKS incorrectly showed superficial venous drainage only, whereas IADSA demonstrated deep venous drainage. The deep draining vein was too small to demonstrate the great vein of Galen in the arterial phase and this small deep draining vein could not be detected on TRICKS.

Arteriovenous malformation grade

AVM detection was graded (range 1 to 5) according to the nidus size, location, and venous drainage route. There was an excellent correlation between IADSA and TRICKS, with discrepancies observed in only 2 cases ($\kappa = 0.89$, **Table 4-3**)

8-4. 【Discussion】

In this study, 3-T TRICKS achieved 96% sensitivity and 100% specificity in both nidus detection and detection of early venous filling (Note that 100% specificity of early venous filling was based on the only one case, so that the perfect value did not necessarily explain or mean the superiority of 3-T TRICKS). Characteristics of AVMs, assessed with the Spetzler-Martin classification according to the TRICKS findings corresponded highly with those obtained with conventional IADSA.

Unenhanced MRA or T2-weighted MRI are very valuable in the assessment of the angioarchitecture of AVMs (25). These techniques are characterized by high spatial resolution; however, they lack the temporal resolution required to evaluate the hemodynamic aspect of AVMs.

Two-dimensional MR DSA has proven effective in the evaluation of AVMs (3, 45, 66, 73) and it offers sufficient temporal resolution for assessment of AVM hemodynamics. However, the spatial resolution of this modality is restricted when

subsecond temporal resolution is obtained. In a previous report of 2D MR DSA with a temporal resolution of 1.05 seconds per dynamic image (45), sensitivity for detection of AVM was 87%, which was lower than my results because of inferior spatial and temporal resolution.

Contrast-enhanced 3D MR DSA generally achieves better spatial resolution at the cost of temporal resolution (16, 20, 32, 37, 43, 53, 68, 70). When the TRICKS technique was first introduced by Korosec and colleagues in 1996 (33), it offered better temporal resolution, but this resolution remained limited at 1.5 T with 1 frame per 1.5 to 1.8 seconds, vs. the 1 frame per 0.3 to 0.5 seconds that is possible with conventional IADSA (19, 43, 69). This resolution was not sufficient for assessment of the short mean transit times of feeding arteries and draining veins in cerebral AVMs (67).

The new generation of 3-T scanners that has been introduced in recent years can offer several significant advantages, especially for MRA (7, 8, 58). First, the increased

signal-to-noise ratio (SNR) improves spatial resolution with a shorter scan time. Second, these machines can give better background suppression of stationary tissues and greater flow enhancement, resulting in vessel-tissue contrast improvement.

My 3-T TRICKS sequence provided a 0.8-second time resolution while preserving high spatial resolution (0.63×0.74 mm^2). TRICKS with this level of in-plane spatial resolution and subsecond temporal resolution has not been reported previously, and I achieved 96% sensitivity and 100% specificity of nidus detection and early venous filling detection with excellent correlation of the Spetzler-Martin grade between TRICKS and IADSA. The 3D acquisition provided other benefits in addition to the high temporal and spatial resolution. In some cases, it was difficult to detect the deep draining vein on TRICKS MIP images because many vessels were overlaid in the sagittal view; however, the deep veins were distinguished from superficial veins on TRICKS source images (**Fig. 4-3**). This contrasts the limited ability to detect vessel

location in 2D MR DSA even with high in-plane spatial resolution.

It must be acknowledged, however, that both the temporal and spatial resolution of TRICKS are inferior to those of conventional IADSA (0.2 × 0.2 mm^2, 1 frame per 0.3 to 0.5 seconds). TRICKS missed very small draining veins in some cases, which again emphasized that conventional IADSA is generally more suitable for pretreatment study of AVMs because the assessment of small vessel branches is essential in choosing the appropriate clinical management (15). However, there are appropriate indications for the noninvasive, radiation-free, and iodinated contrast agent-free MR DSA, particularly for screening and follow-up. For screening, such as in the case of young patients with intracranial hemorrhage, early venous filling is often the key diagnostic finding indicating the presence of an AVM (3), and for follow up, which requires repeated evaluations (44, 47), assessment of patency and nidus character is necessary (40). In these cases, early venous filling assessment and the Spetzler-Martin

classification take precedence, and the assessment of small vessels and the number of vessels may not be as important as in the pretreatment evaluation. Although larger trials are still needed for prospective evaluation of the diagnostic accuracy of TRICKS at 3-T, my results indicate a high correlation of TRICKS with IADSA in terms of Spetzler-Martin grade as well as 96% sensitivity and 100% specificity of nidus and early venous filling detection. This finding indicates that the TRICKS sequence may be a suitable alternative to conventional IADSA in selected cases of screening and follow-up in patients with AVMs.

There are limitations to the implementation of TRICKS. First, artifacts may occur at the edge of enhancing vessels due to the technical character of TRICKS (17). Although this factor did not have a great influence on early venous filling assessment and Spetzler-Martin classification in the present study, artifacts may hinder the assessment of small vessels. Second, the total slice thickness of 6.4 cm sometimes fails to include

some of the main components, such as the superior sagittal sinus or sigmoid sinus, depending on the nidus location. Appropriate FOV setting can prevent misinterpretation until faster imaging techniques are developed that enable obtaining a greater slice thickness. Third, in MR DSA, basically only 1 plane of projected images can be obtained in a single contrast-injection sequence. The 3D acquisition technique TRICKS enables image reconstructions in any direction desired, but a 4.0-mm slice thickness (with zero fill interpolation processing) is so inferior to the in-plane spatial resolution (0.63 × 0.74 mm) that the reconstructed images are rather rough compared with the original projected images. Although it is actually possible to assess depth information from TRICKS source images or stereoscopic visualization of the MIP images, if the images are not acquired in the proper orientation, the observer might find the evaluation of detailed hemodynamic information more difficult. In the present study, I used the sagittal plane for image acquisition in all patients because previously

obtained unenhanced MR images led us to judge that to be appropriate, and I was able to assess all AVMs well. It might be necessary to check the size and location of AVM nidi on unenhanced MRI sequences, such as T2WI, before starting TRICKS to prevent an inappropriate plane setting. Fourth, items such as hematomas that have short signals on T1WI are depicted as high intensity on nonsubtracted images in TRICKS, as on a T1WI. This sometimes makes the assessment of the vessel route difficult. On subtracted TRICKS images, however, the high signal of the hematoma (or other confounder) is subtracted together with the other background signals, and so should not affect the assessment of AVM.

A limitation to my study is that I did not conduct examinations in a control group of patients without AVMs to rule out observer bias. However, I believe this bias was reduced by including the patients with occluded AVMs.

8-5.【Conclusion】

Time-resolved contrast-enhanced 3D MRA at 3-T can provide important information about AVM such as early venous filling and Spetzler-Martin classification, which corresponds strongly with the findings of IADSA. Although this is a preliminary study, the results indicate that time-resolved contrast-enhanced 3D MR A at 3-T has the potential to replace conventional IADSA at screening or follow-up for patients with AVMs.

9. Discussion of this Study

The results of the basic experiments presented here were as expected based on the principles of MRI. By adjusting imaging parameters based on these results, I was able to obtain image quality appropriate for imaging diagnostics, and preliminary results of clinical application of these methods indicated that they were able to evaluate intracranial hemodynamics and that they have the potential to contribute to a meaningful reduction in the number of conventional X-ray IADSA procedures that are required for safe and effective evaluation and follow up of patients with AVM and other potentially life-threatening intracranial vascular lesions. In the future, MR-guided intravascular procedures that do not expose patients to X-rays may also be made possible by expanding these applications to intra-arterial techniques.

My novel method of MRDSA had an unexpected limitation, the recently-recognized complication of the gadolinium contrast agent. Over the past several years, researchers have correlated the development of nephrogenic systemic fibrosis (NSF) with the

increasing use of gadolinium-based MRI contrast agents in patients with kidney disease. Therefore, we cannot easily adopt MRDSA alternating X-ray IADSA.

10. Conclusion

MRDSA can produce vascular images with adequate spatial resolution and temporal resolution that are easy to interpret without the use of special technology or software. MRDSA provides information on hemodynamics that cannot be obtainable with conventional MRI methods, and it is a useful diagnostic tool, particularly in the screening and follow-up of patients with AVM or other intracranial vascular disorders. MRDSA is more routinely performed in flagship hospitals than when it was studied. I hope that MRDSA as a means of easily obtaining hemodynamic information will become further widespread especially in community hospitals.

11. Tables and Figures

Table 2-1. Detection of AVMs as early venous filling on 2D MRDSA

AVM	Early venous filling present	Absent or equivocal	Total
Yes	48	7	55
No	0	23	23
Total	48	30	78

Table 2-2. Detection of AVMs as nidus flow void on T2-weighted images

AVM	Flow void present	Absent or equivocal	Total
Yes	44	11	55
No	2	21	23
Total	46	32	78

Table 2-3. Comparison of T2-weighted images and 2D MRDSA

Early venous filling on 2D MRDSA	Nidus flow void on T2-weighted images		
	Present	Absent or equivocal	Total
Present	44	4	48
Absent or equivocal	2	28	30
Total	46	32	78

Table 3-1. Mean rank of visualization of normal cranial vessels (n=24, 5-cm slice thickness)

Larger vascular structures tended to be depicted more clearly than smaller structures

Vessel	Mean rank	Cohen's kappa value
ICA	**3.00**	**1.00**
Opthalmic artery	**1.67**	**0.93**
ACA (A1, A2)	**2.71**	**0.66**
ACA (A3, A4)	**2.33**	**0.71**
MCA (M1, M2)	**2.63**	**0.73**
MCA (M2, M4)	**2.20**	**0.70**
VA	**2.96**	**1.00**
BA	**2.88**	**1.00**
PCA	**2.25**	**0.66**
SSS	**3.00**	**1.00**
Straight sinus	**2.92**	**0.66**
Deep cerebral veins	**2.83**	**0.83**
Transverse/sigmoid	**2.79**	**0.71**
Jugular vein	**2.79**	**0.64**

Table 3-2. Correlation between vascular visualizations demonstrated on 2D MRDSA with ASSET and those on 2D MRDSA without ASSET (n=10)

		Rank on 2D MRDSA without ASSET			
		1	2	3	Total
Rank on 2D MRDSA with ASSET	1	5	1	6	12
	2	0	13	22	35
	3	0	1	92	93
	Total	5	15	120	140

Correlation was performed by Spearman rank test. Correlation value was 0.55 ($P<0.0001$). Rank for vascular visualization defined as follows: 1 = not seen, 2 = seen but deteriorated and 3 = clearly seen.

Table 4-1. Summary of characteristics in 31 patients with AVMs

Charasteristic	No. of Pathients (%)
AVM location	
supratentorial	**23 (74)**
frontal lobe	**2 (6)**
temporal lobe	**6 (19)**
parietal lobe	**7 (23)**
occipital lobe	**5 (16)**
corpus callosum	**2 (6)**
thalamus/basal ganglia	**1 (3)**
infratentorial	**4 (13)**
pons/medulla	**1 (3)**
cerebellum	**1 (3)**
cerebellopontine angle	**2 (6)**
angiographically occluded	**4 (13)**

*There were 14 men and 17 women with a mean age of 38.2±12.5 years (range 16-74 years).

Table 4-2. Summary of conventional catheter angiography and TRICKS findings for the Spetzler-Martin classification of 25 patients*

Parameter	No. of AVMs	
	Catheter Angiography	TRICKS
size (cm)		
< 3	**11**	**12**
3-6	**12**	**11**
> 6	**2**	**2**
location		
eloquent	**12**	**12**
noneloquent	**13**	**13**
Venous drainage		
superficial	**11**	**12**
deep	**14**	**13**

*The case with small dilated draining vein only and the case in which TRICKS failed to include the great vein of Galen in the FOV were excluded from Spetzler-Martin classification assessment.

Table 4-3. Comparison of Spetzler-Martin grades as assessed with TRICKS and conventional catheter angiography in 25 patients*

TRICKS Grade	Catheter Angiography Grade				
	Ⅰ	Ⅱ	Ⅲ	Ⅳ	Ⅴ
Ⅰ	3	1	0	0	0
Ⅱ	0	8	1	0	0
Ⅲ	0	0	7	0	0
Ⅳ	0	0	0	3	0
Ⅴ	0	0	0	0	2

* κ =0.89

Fig. 1-1. Phantom used to examine slice thickness.

Tubes filled with diluted contrast agent were placed at 5-mm intervals on both sides of a cylindrical object. Imaging was performed with the MRDSA pulse sequence at slice thicknesses that varied from 1 cm to 10 cm. The signal intensities of the tube images were measured on the slice profiles that were obtained.

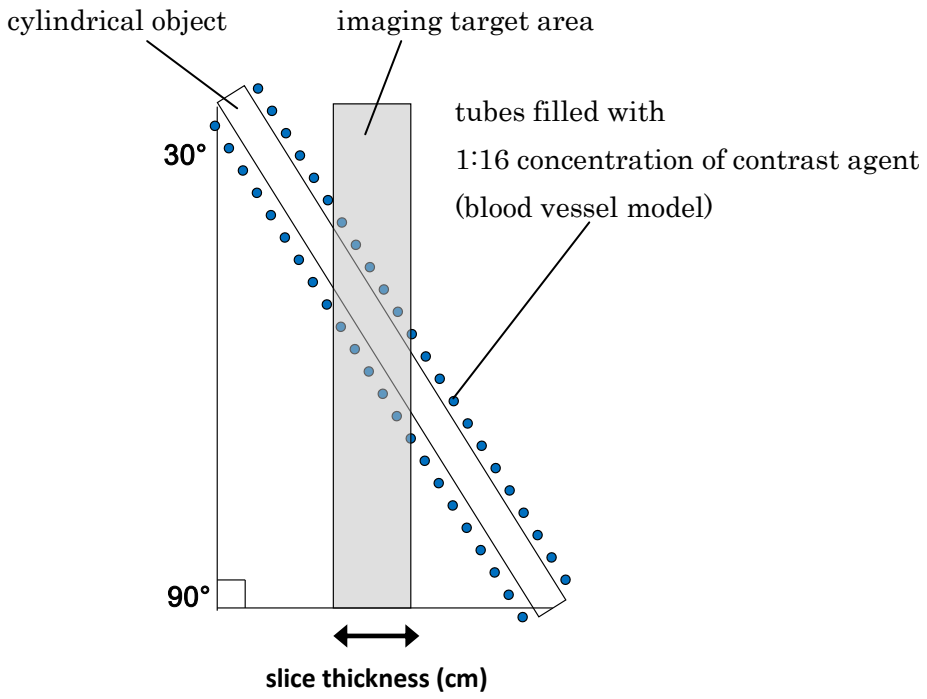

Fig. 1-2. Changes in SSR when echo time (TE) is varied.

The vertical axis is SSR and the horizontal axis is TE (msec). The signal intensity of the contrast agent increased as TE was shortened, while the signal intensity of the brain matter did not change. Thus, the SSR was inversely related to TE.

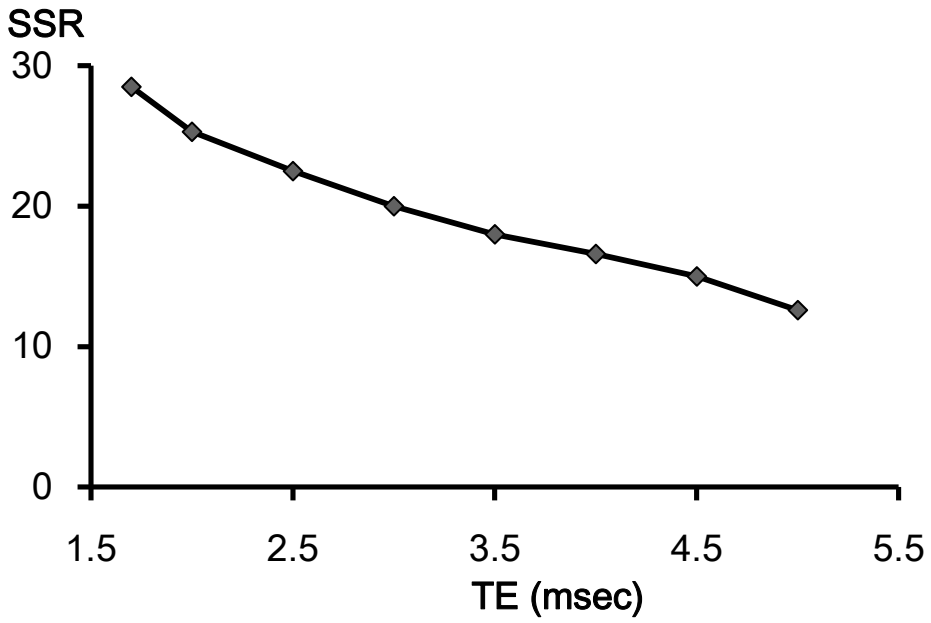

Fig. 1-3. Changes in SSR when repetition time (TR) is varied.

The vertical axis is SSR and the horizontal axis is TR (msec). The signal intensity of the contrast agent decreased slightly as TR was shortened, while the signal intensity of the brain matter decreased greatly. Thus, the SSR was inversely related to TR.

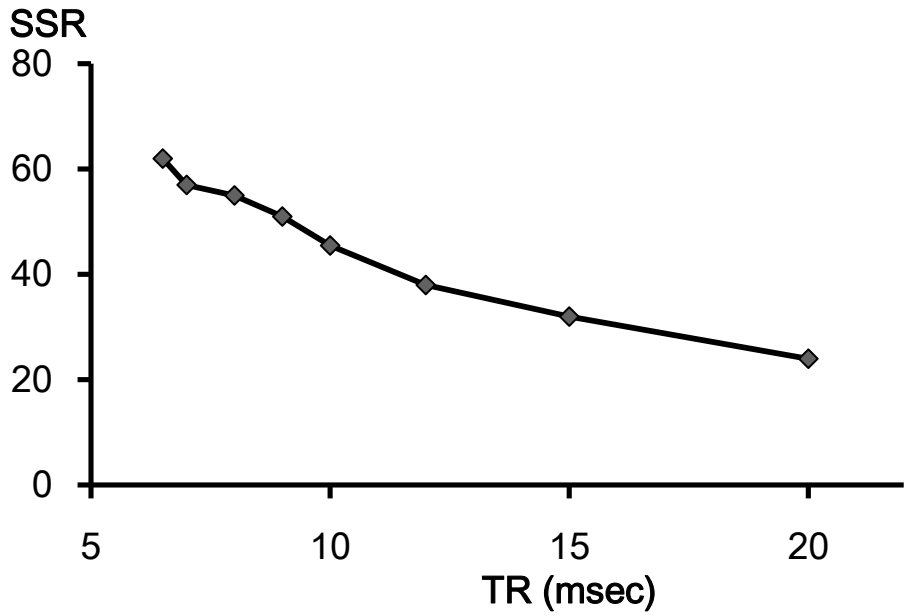

Fig. 1-4. Changes in SSR when flip angle is varied.

The vertical axis is the SSR and the horizontal axis is the flip angle (degrees). The signal intensity of the contrast agent decreased markedly as the flip angle declined and the signal intensity of the brain matter increased. Thus, the SSR was directly related to flip angle.

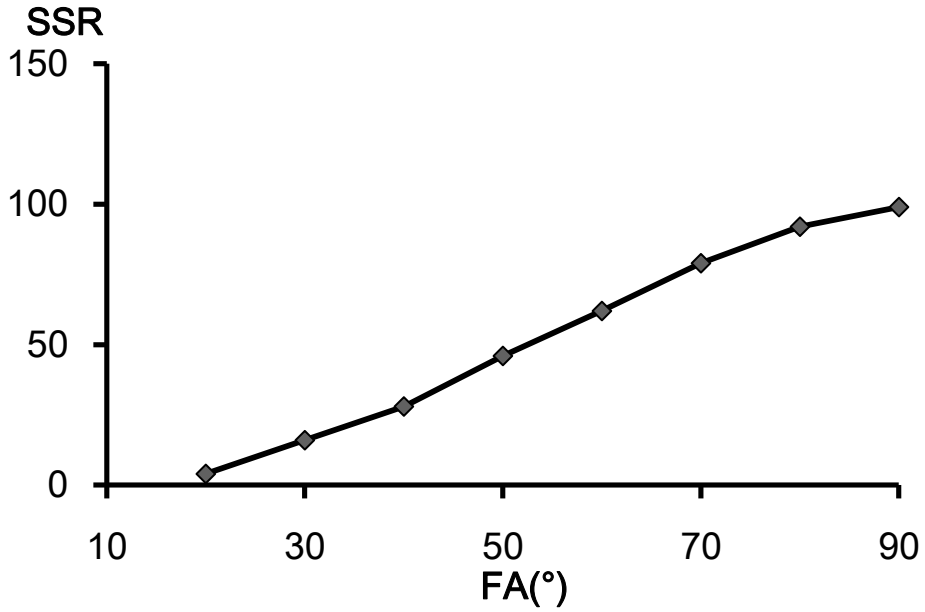

Fig. 1-5. Changes in signal intensity (SI) when concentration of contrast agent is varied.

The SI of the contrast agent was highest at a dilution of around 1:8, and decreased with both higher and lower concentrations.

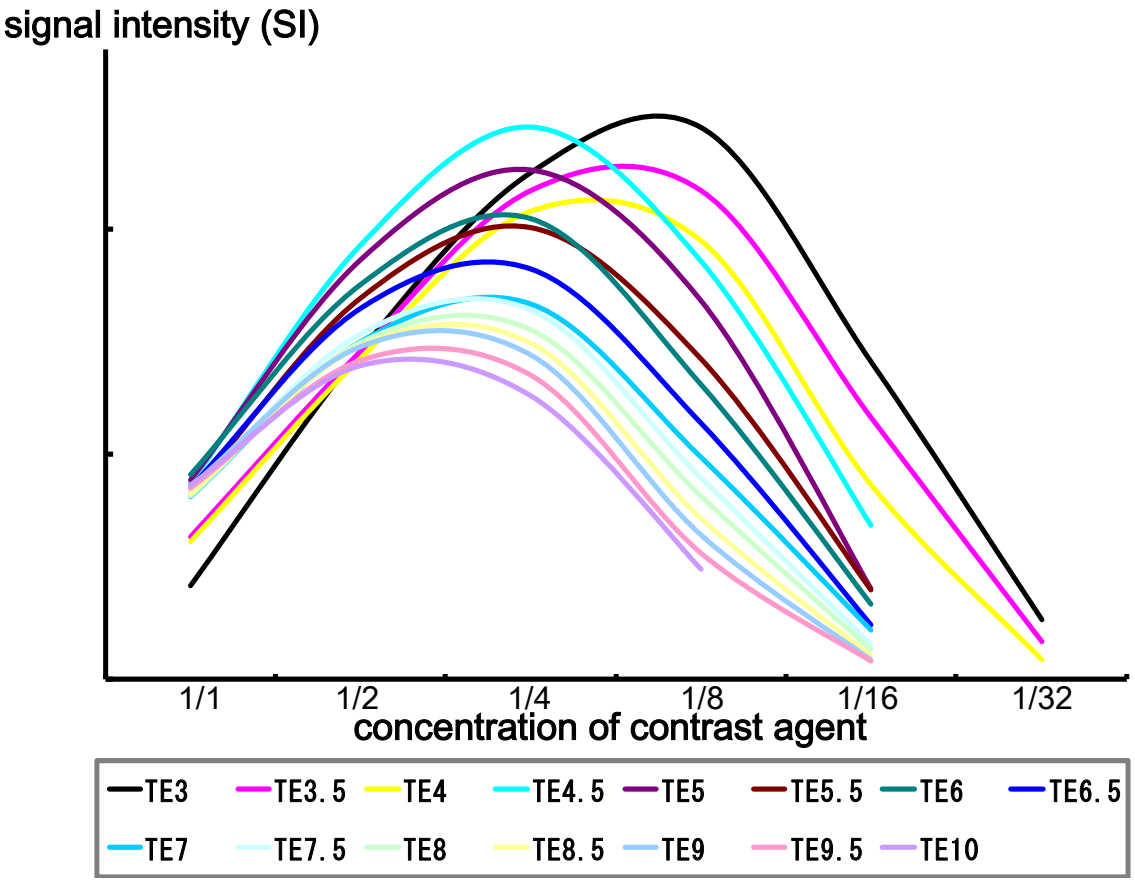

Fig. 1-6. Slice profile investigation

The blue lines show the slice profiles obtained from actual imaging at certain thickness settings. The yellow shading indicates the theoretical slice profile for an RF pulse obtained in an ideal state. In practice, signals greater than the established thickness were obtained. The left-right differences were thought to be due to variations in the position from the center of the static magnetic field.

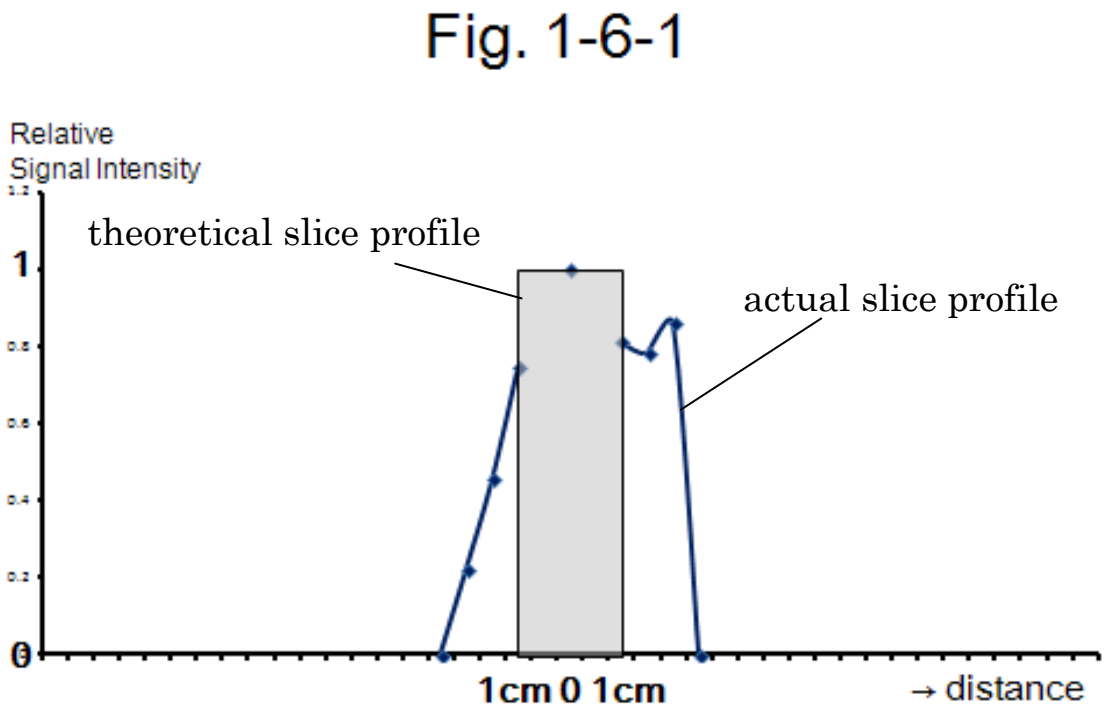

Fig. 1-6-2

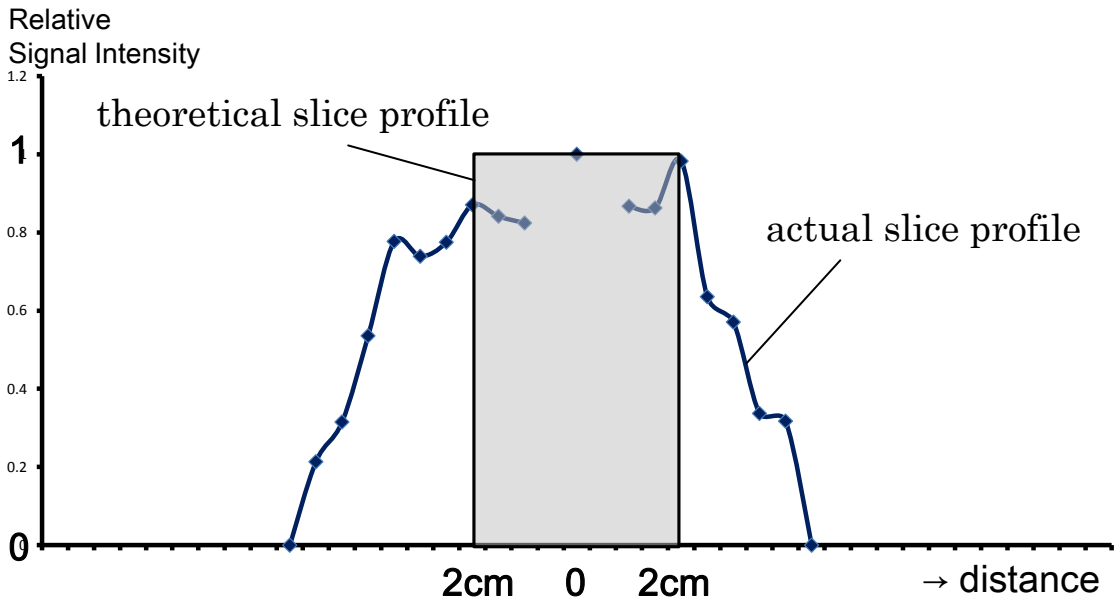

Fig. 1-6-3

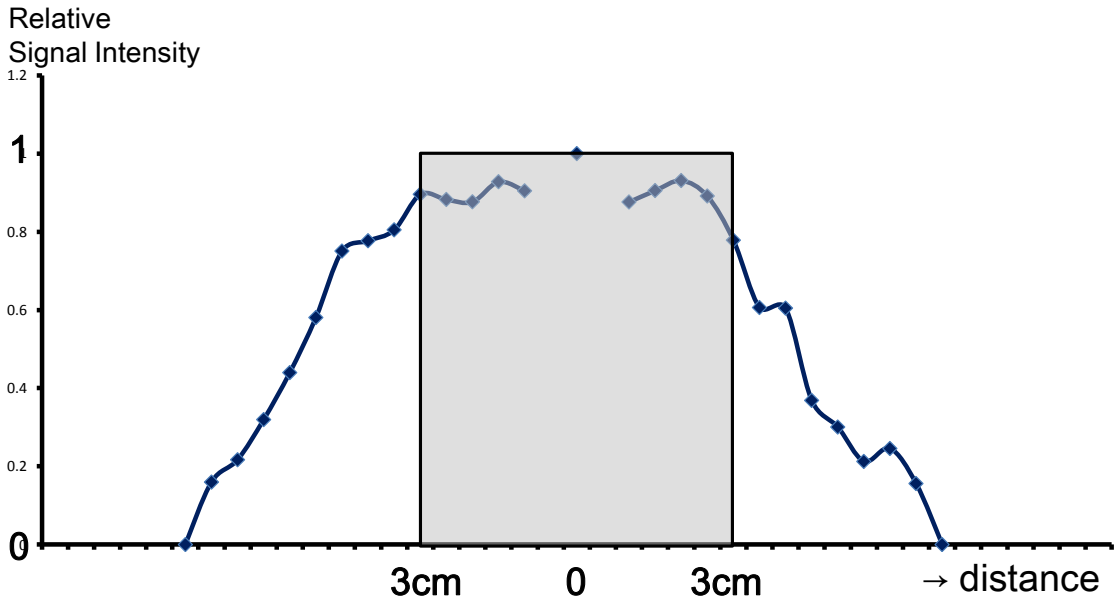

Fig. 1-6-4

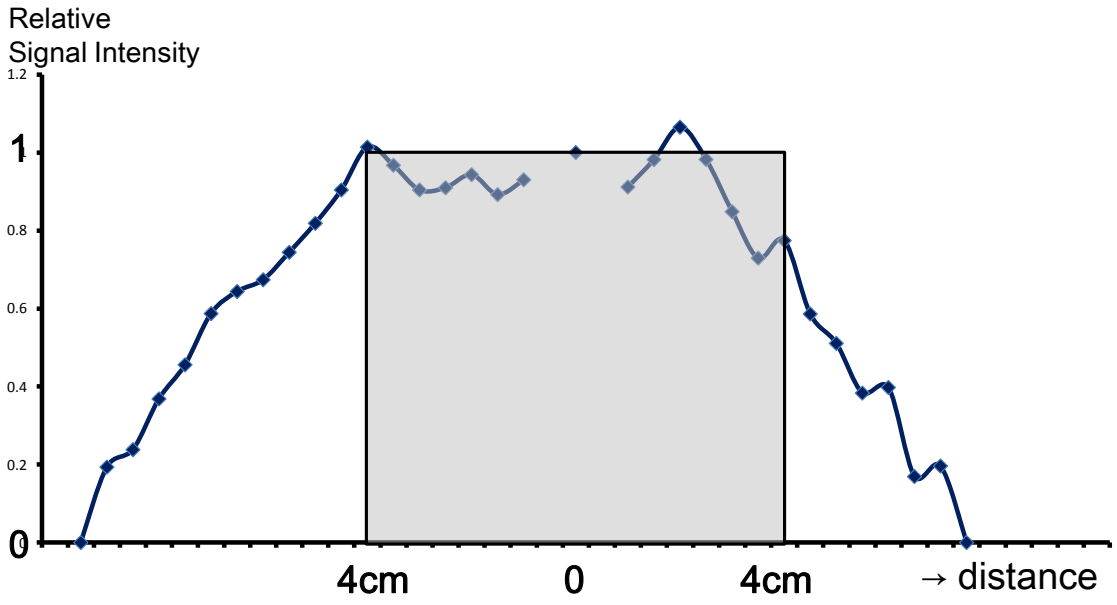

Fig. 1-6-5

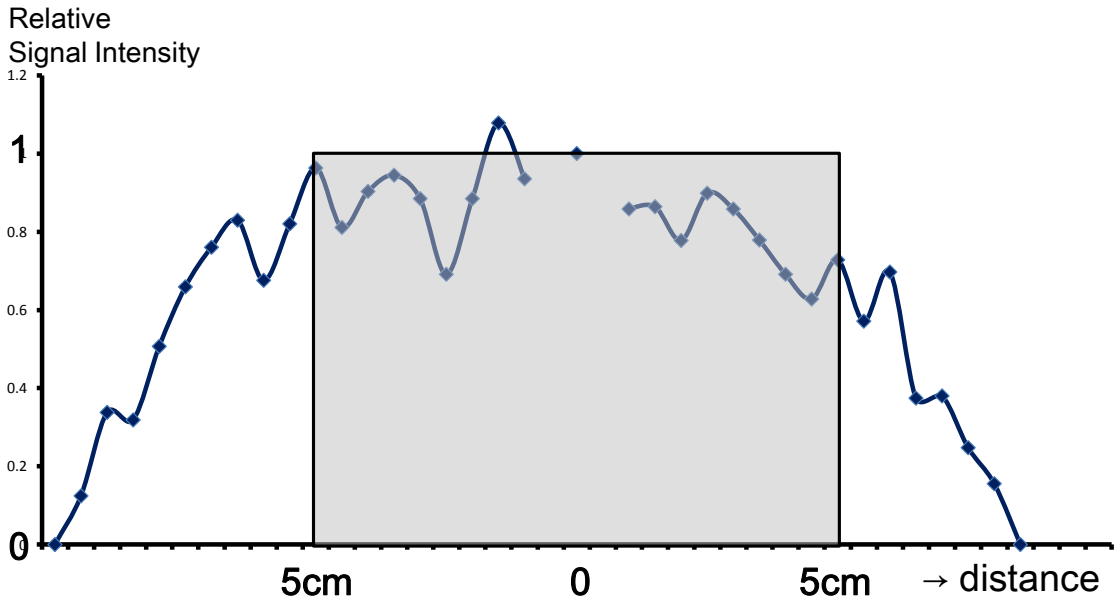

Fig. 1-6-6

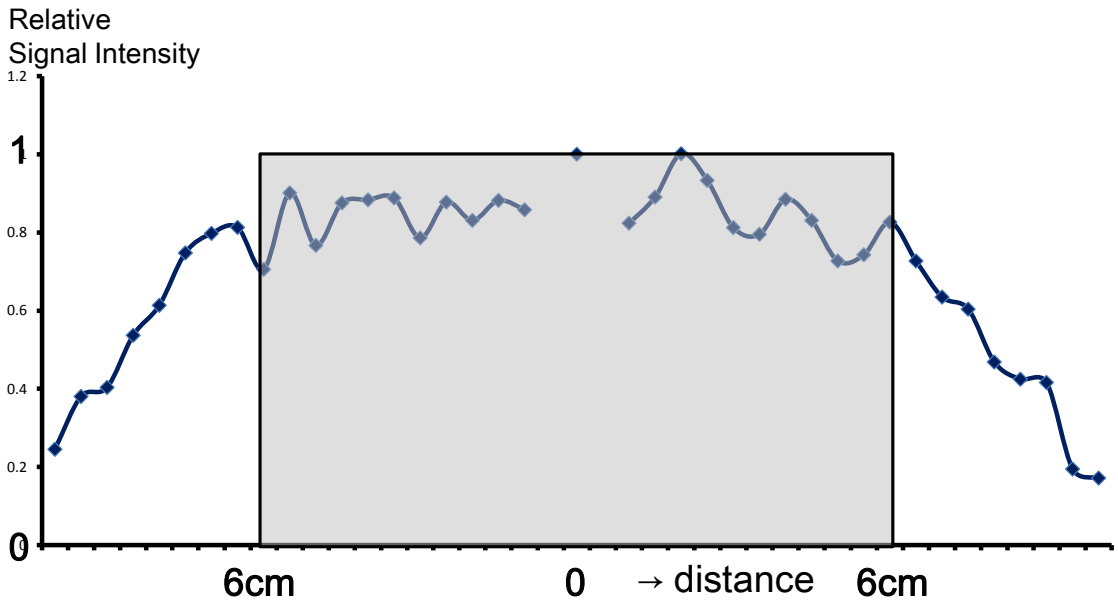

Fig. 1-6-7

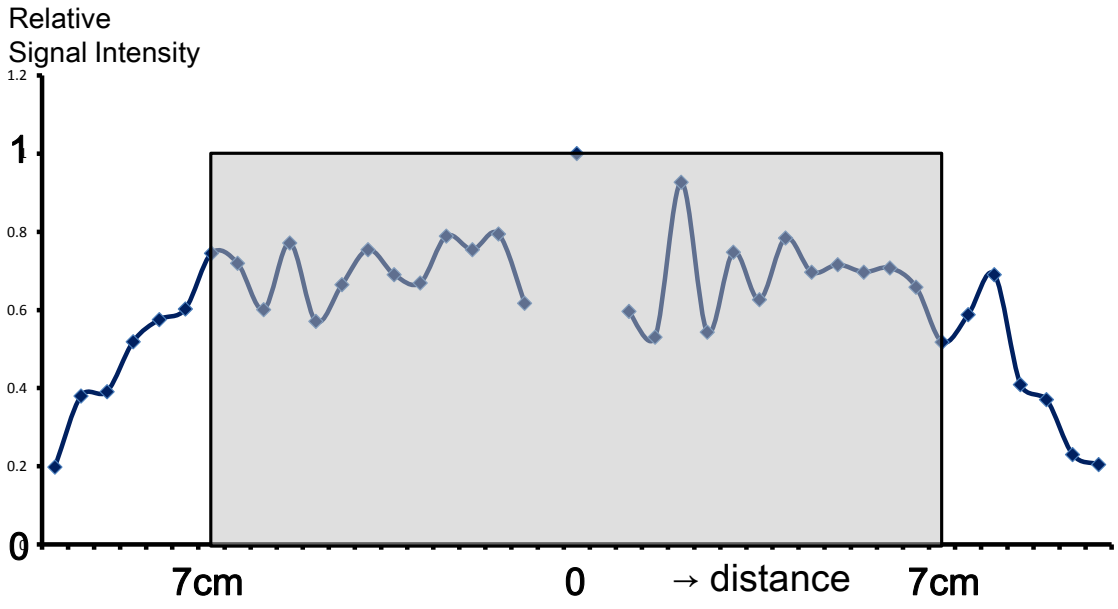

Fig. 1-6-8

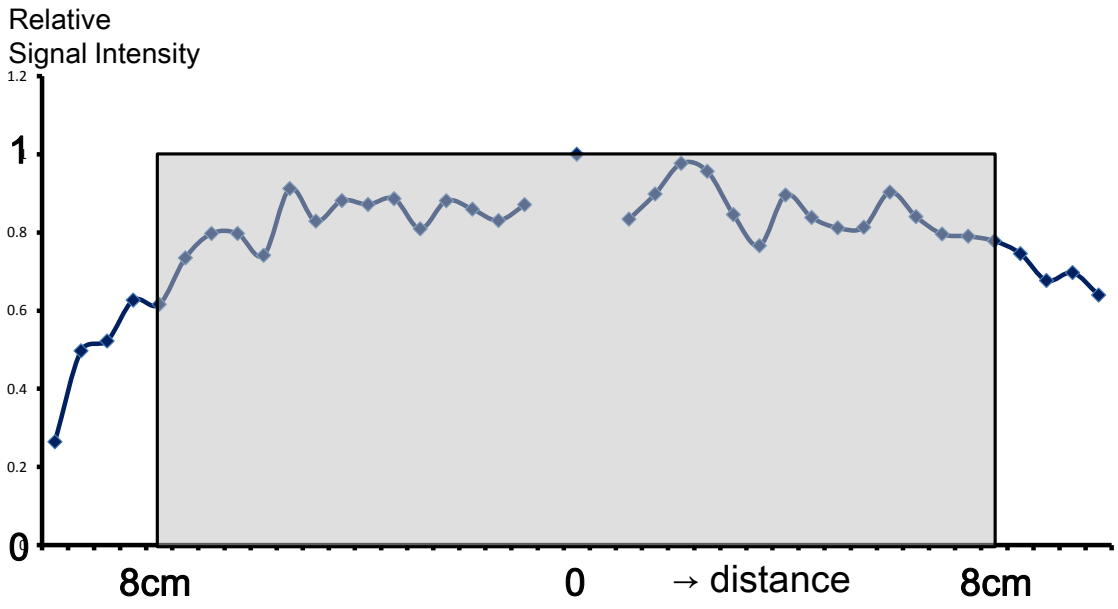

Fig. 1-6-9

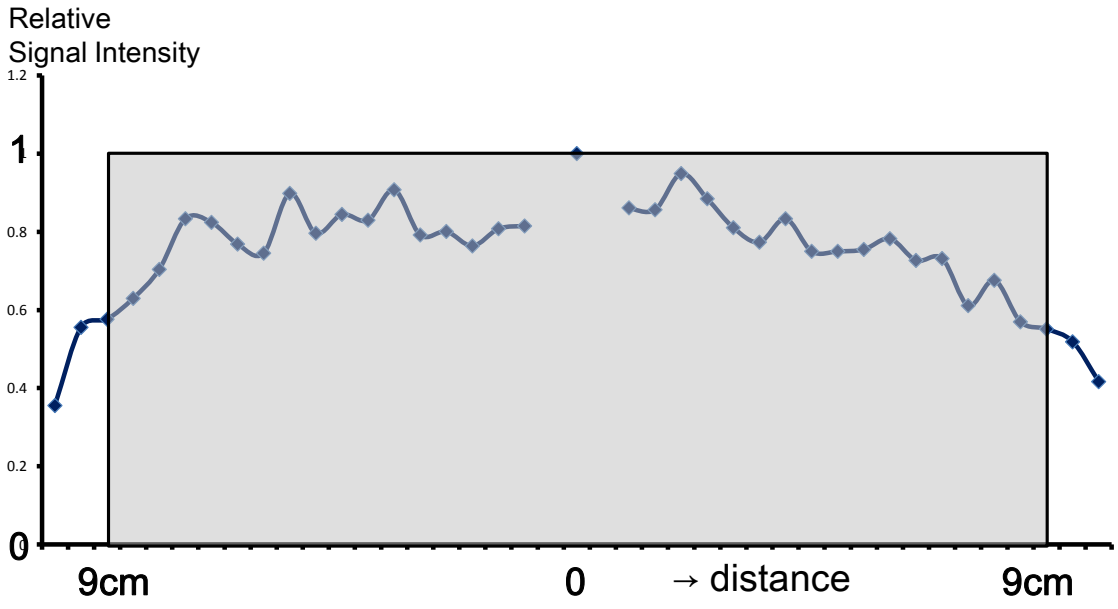

Fig. 1-6-10

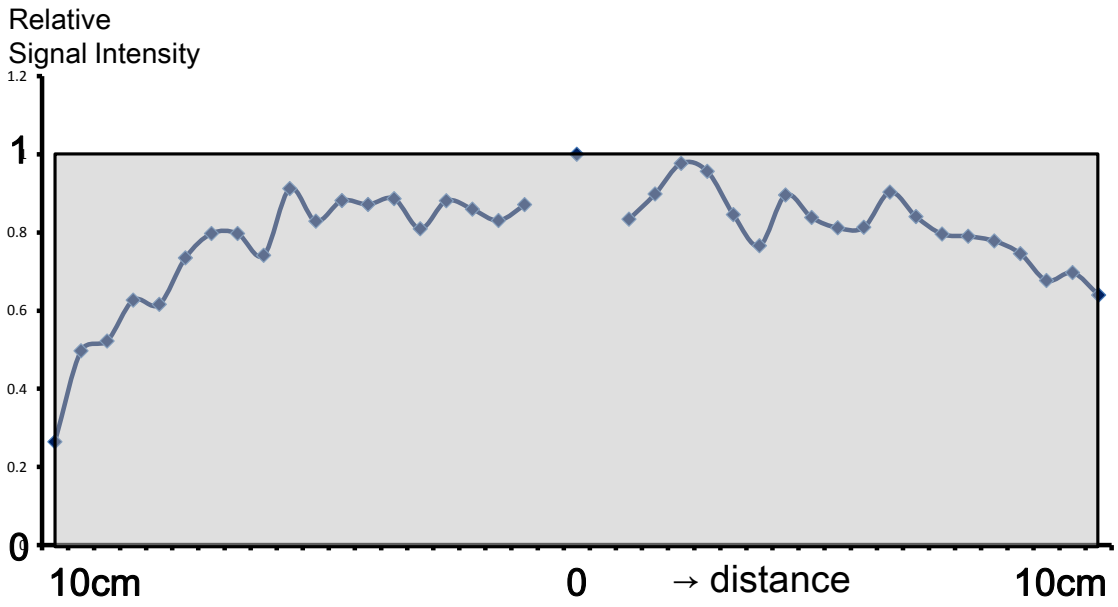

Fig. 1-6-11

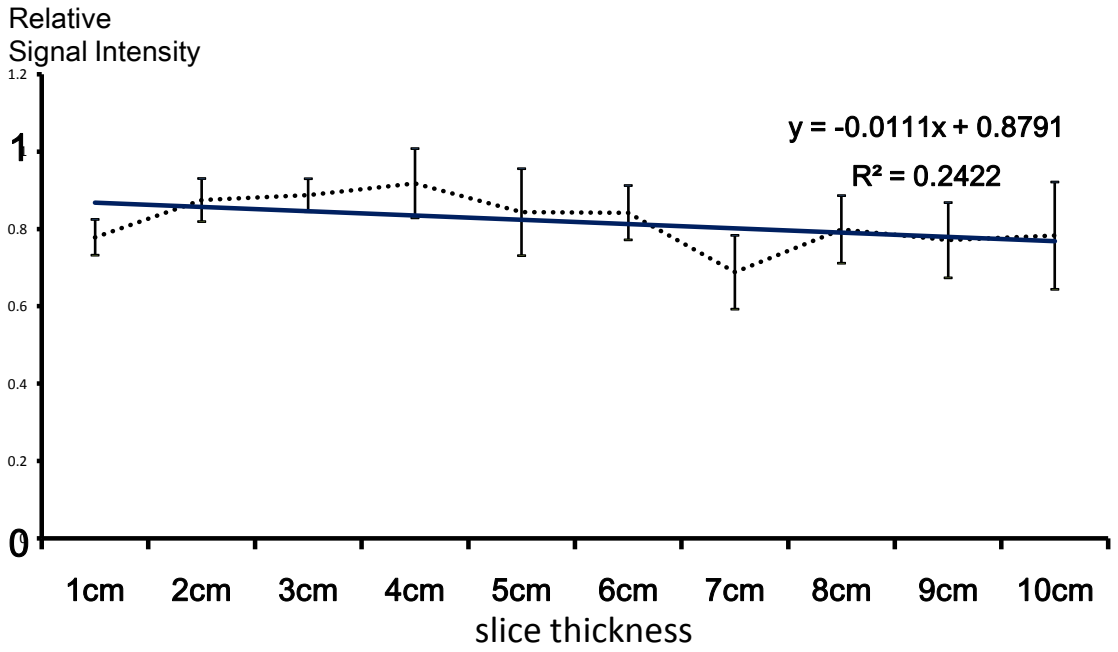

Fig. 2-1.

A 33-year-old man with left frontal AVM. Pre-gamma-knife study.

a) The conventional catheter angiogram shows an AVM fed by frontal branches of the left middle cerebral artery and draining into the superior sagittal sinus via a dilated vein of Trolard with large varix and other draining veins. b) T2-weighted MR image displays nidus flow voids in the left frontal lobe. c–e) Gray-scale-reversed 2D MRDSA images in the sagittal plane separately describe each component of the AVM, feeding vessels, nidus stains, draining vessels, and Trolard varix in order with time.

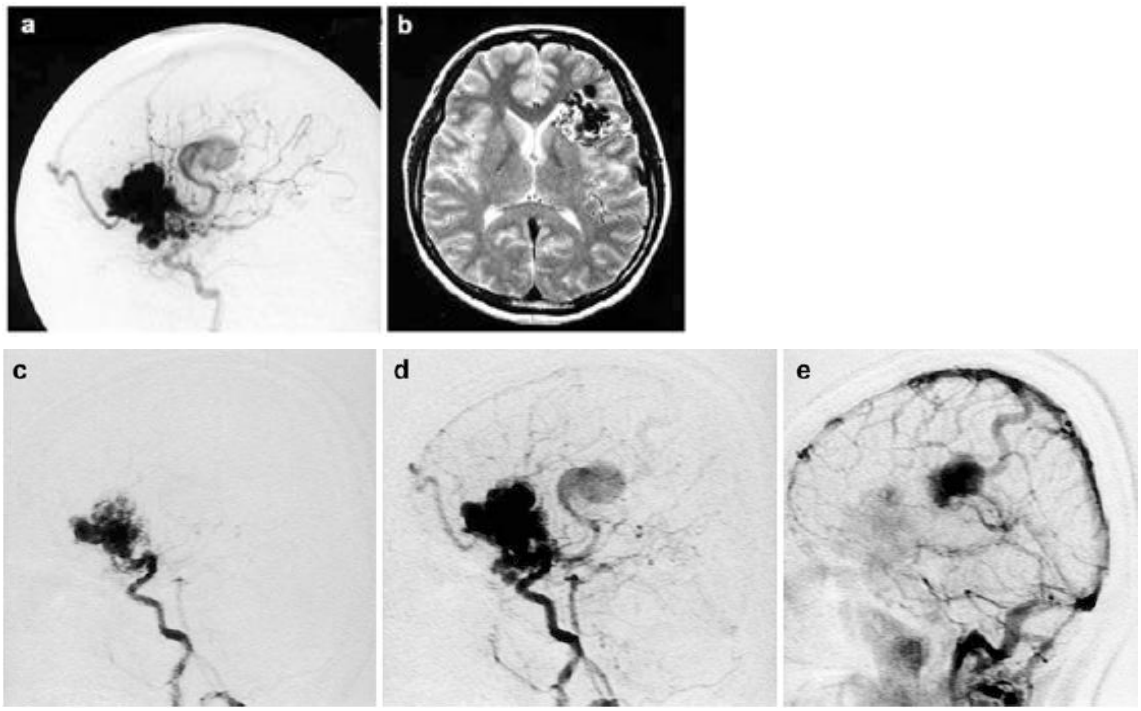

Fig. 2-2.

A 41-year-old man with left frontal AVM. Pre-gamma-knife study.

a) The conventional catheter angiogram reveals an AVM fed by the left posterior internal frontal artery draining to the superior sagittal sinus. b) T2-weighted MRI exhibits nidus flow voids in the left frontal lobe. c–e) 2D MRDSA images clearly describe each component of the AVM in order with time.

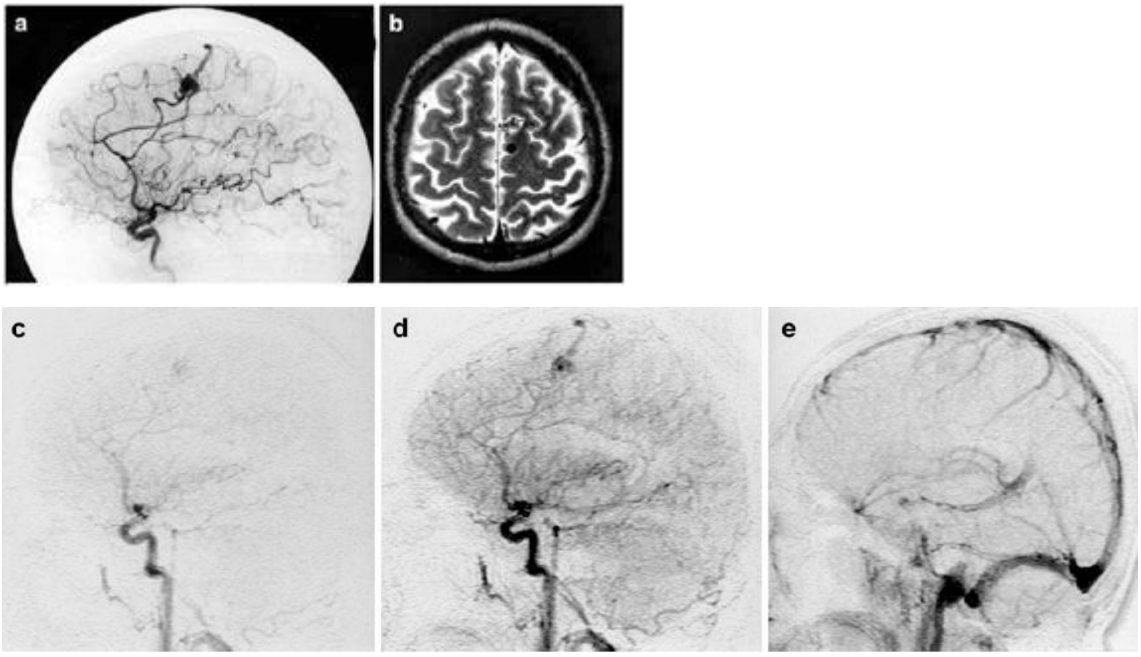

Fig. 2-3.

A 47-year-old woman with right occipital AVM. Post-gamma knife study.

a) Pre-gamma knife conventional catheter angiogram shows an AVM fed by the angular artery of the right middle cerebral artery and the parieto-occipital artery of the right posterior cerebral artery (not shown). It drains into the superior sagittal sinus. b) T2-weighted MRI performed 32 months after gamma-knife radiosurgery cannot discern an obvious nidus flow void; however, a slightly heterogeneous hypointense dot lacking continuity is displayed (arrow). c–e) The 2D MRDSA images obtained simultaneously demonstrated the nidus and draining vessels (arrows). In this case, 2D MRDSA proved superior to T2-weighted MRI.

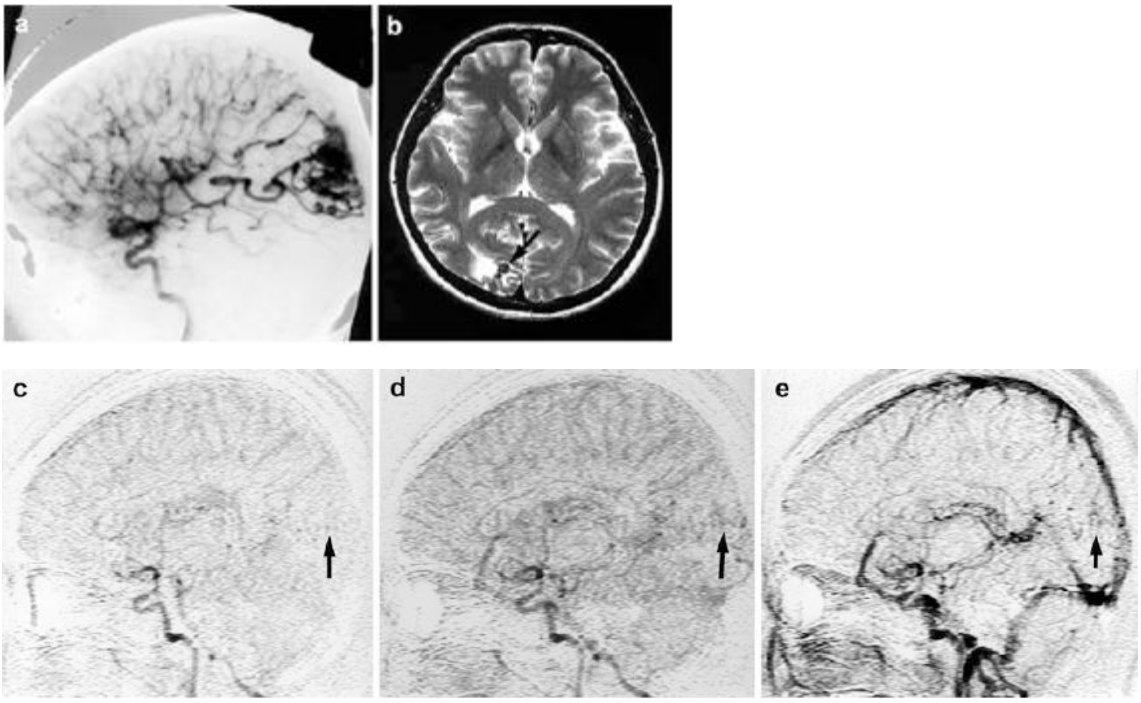

Fig. 3-1.

A 29 year-old man with a frontal AVM.

a–c) Sequential 2D MRDSA images with ASSET reveal an AVM fed by branches of the middle cerebral artery draining into the superior sagittal sinus via superior cerebral veins and into the sphenoparietal sinus via the superficial middle cerebral vein. The direction of early venous filling can be perceived more readily on these images than on (d) and (e) due to improved temporal resolution. d, e) Sequential images of conventional 2D MRDSA. (d) and (e) correspond in time to (a) and (c), respectively. f) Catheter angiogram obtained at the corresponding arterial phase.

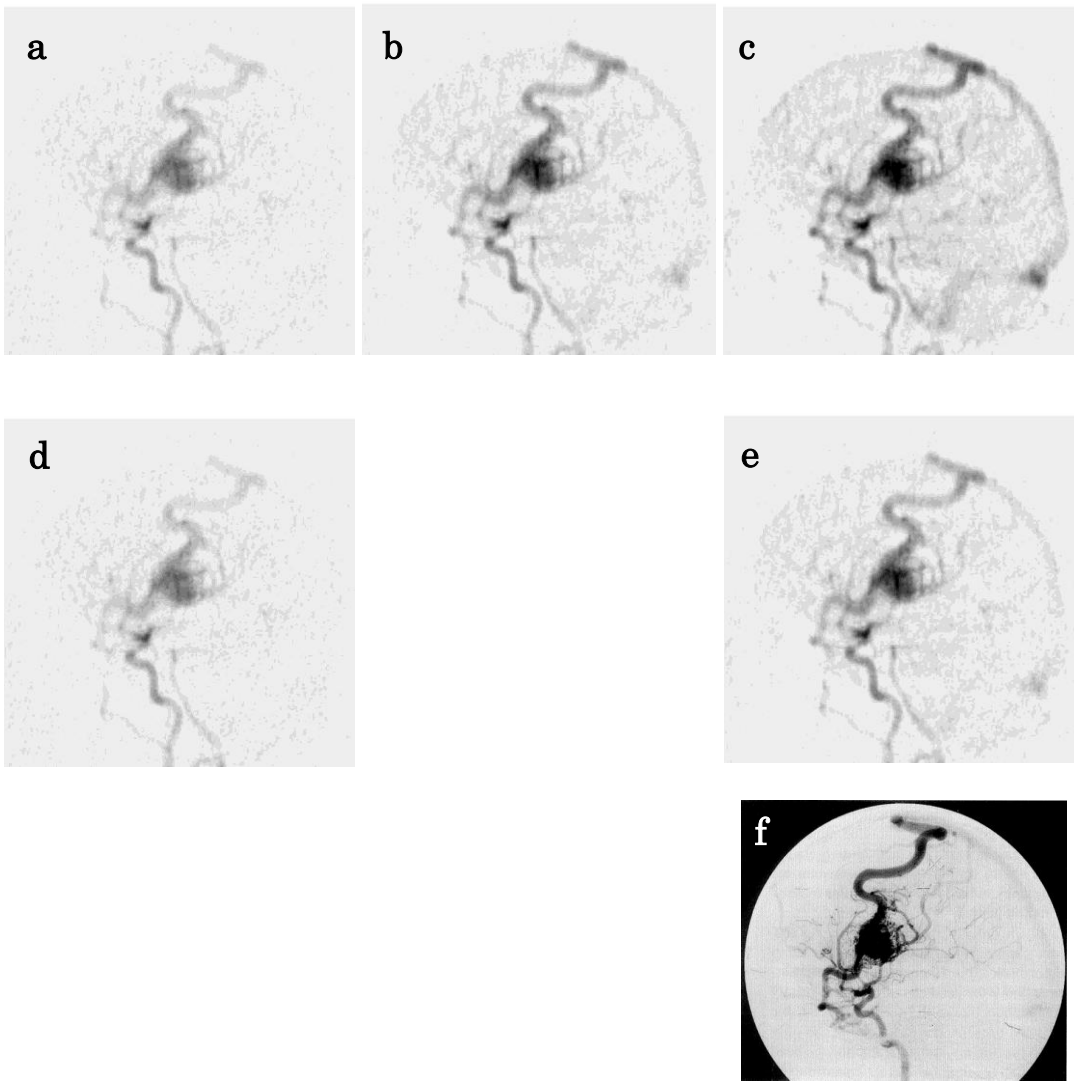

Fig. 3-2.

A 42 year-old man with temporal AVM.

a) The 2D MRDSA with ASSET image shows an AVM in the temporal area posteriorly overlapped by an aliased spot of nasal mucosa (arrows). b) No such aliased spot is visible on the conventional 2D MRDSA image.

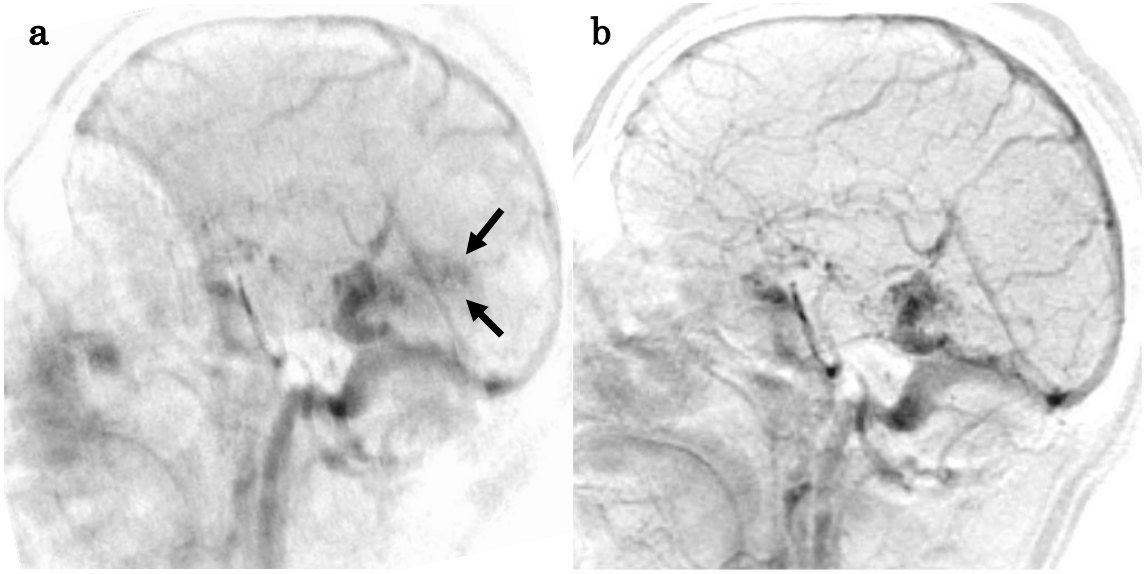

Fig. 4-1.

a, b) Conventional catheter angiograms of the right common carotid artery showing a nidus in the right corpus callosum fed by the branches of the right anterior cerebral artery. The dilated draining vein (arrow) is demonstrated in the arterial phase. c, d) Maximum intensity projection images obtained with TRICKS. The small nidus (arrows) and the early filling of the draining vein (arrowhead) are clearly demonstrated.

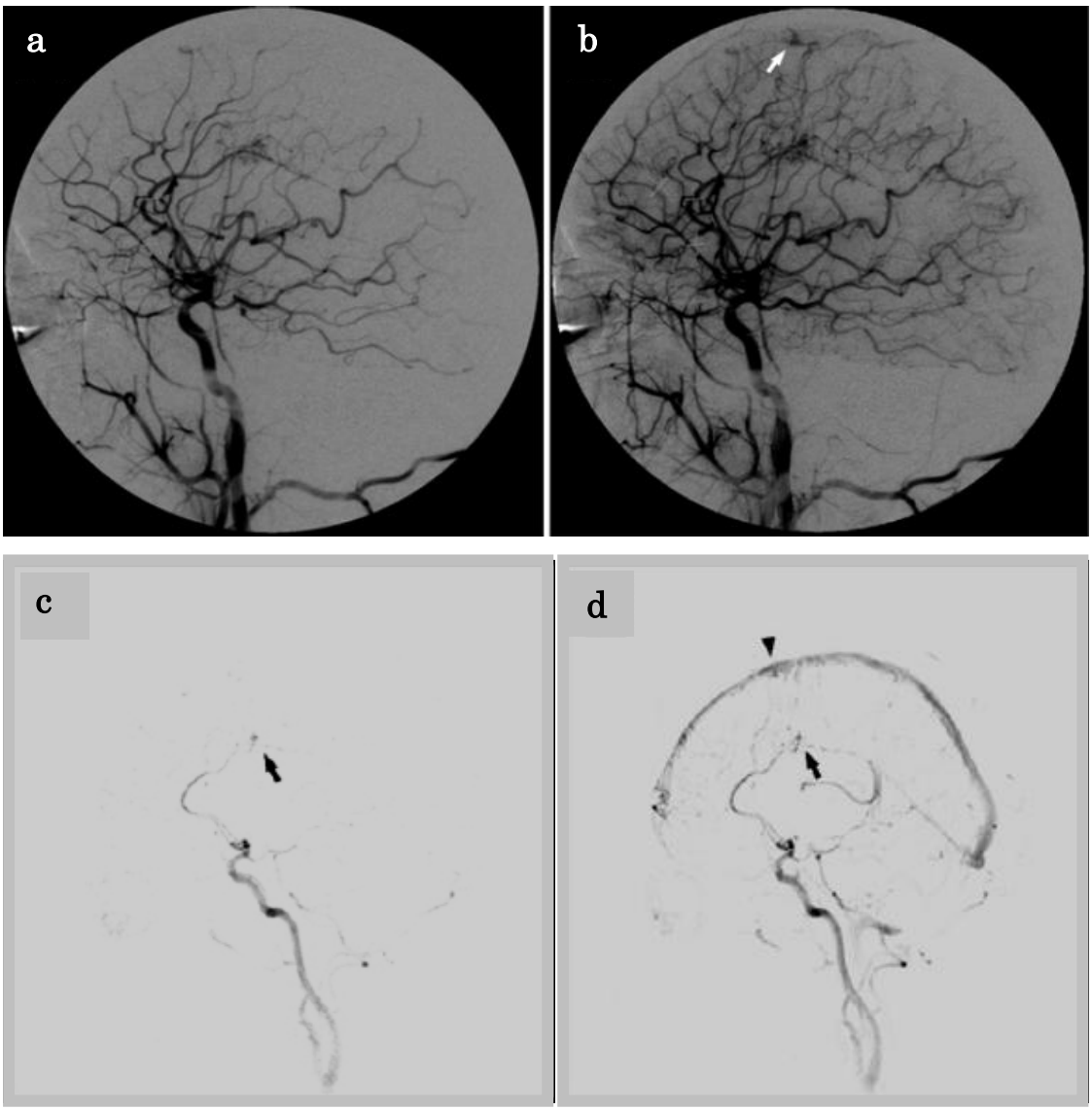

Fig. 4-2.

a, b) Conventional catheter angiograms of the right common carotid artery showing a nidus in the right temporooccipital lobe with early filling of the right transverse sinus. c–e) Maximum intensity projection images obtained with TRICKS. The nidus is easily detected, and the right transverse sinus and sigmoid sinus are demonstrated in the early phase.

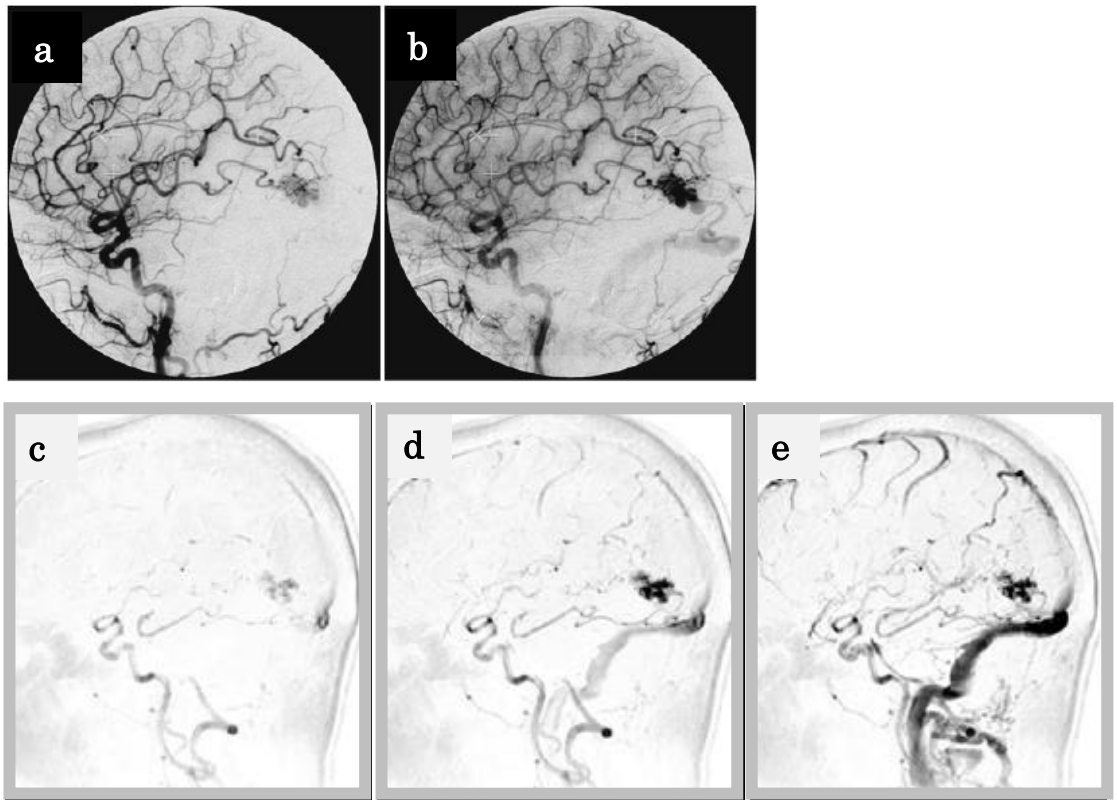

Fig. 4-3.

a, b) Conventional catheter angiograms of the left internal carotid artery showing a large nidus in the left occipital lobe fed by the left middle temporal artery. On the oblique view, a vein draining into the great vein of Galen is seen (arrow); note that this is difficult to evaluate on the lateral view. c–e) Maximum intensity projection images of TRICKS showing that the deep drainage route is difficult to detect. f, g) The source images of TRICKS. The deep draining vein is clearly shown (arrows).

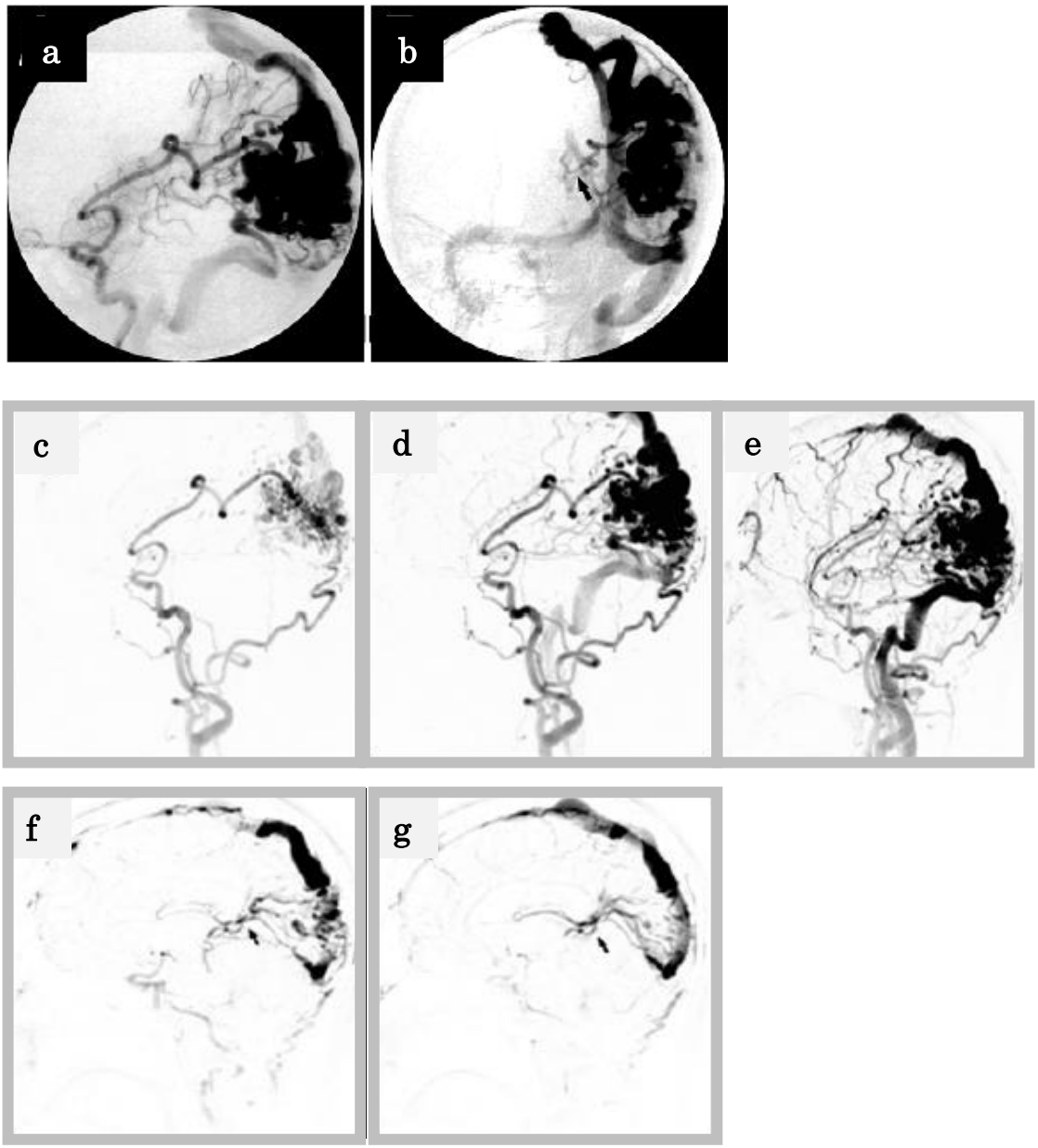

12. Appendices

Appendix 1

Basic concepts of MRDSA

MRDSA images are acquired by administering a contrast agent during continuous imaging measured in seconds. From these, a raw image in which the contrast agent has not yet arrived is used as the mask image, and the background is erased by subtracting the mask image from several dozen subsequent images, which produces a difference image similar to X-ray DSA imaging.

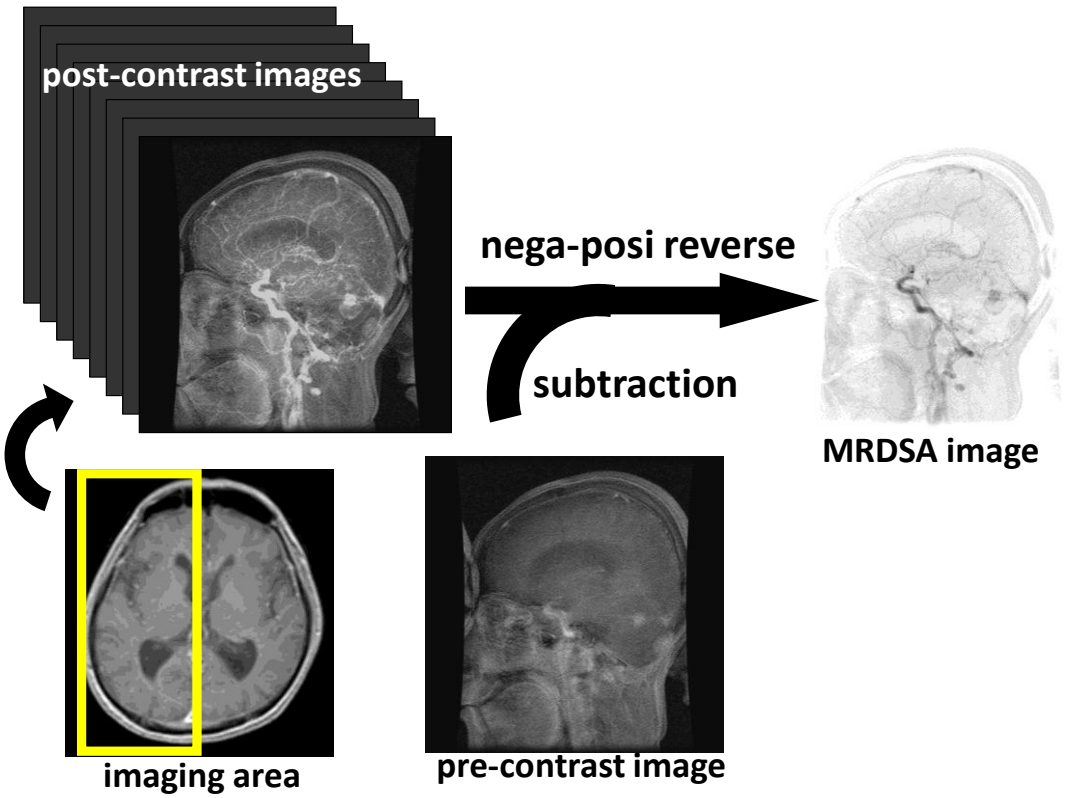

Appendix 2

Basic concepts of parallel imaging (ASSET)

Prarallel imaging is a fast imaging technique. In this technique, parallel data sampling is performed by multiple small phased-array coils that have different sensitivity distributions. The parallel data (i.e. aliasing artifact) is expanded by the sensitivity difference of each coil and changed into proper images.

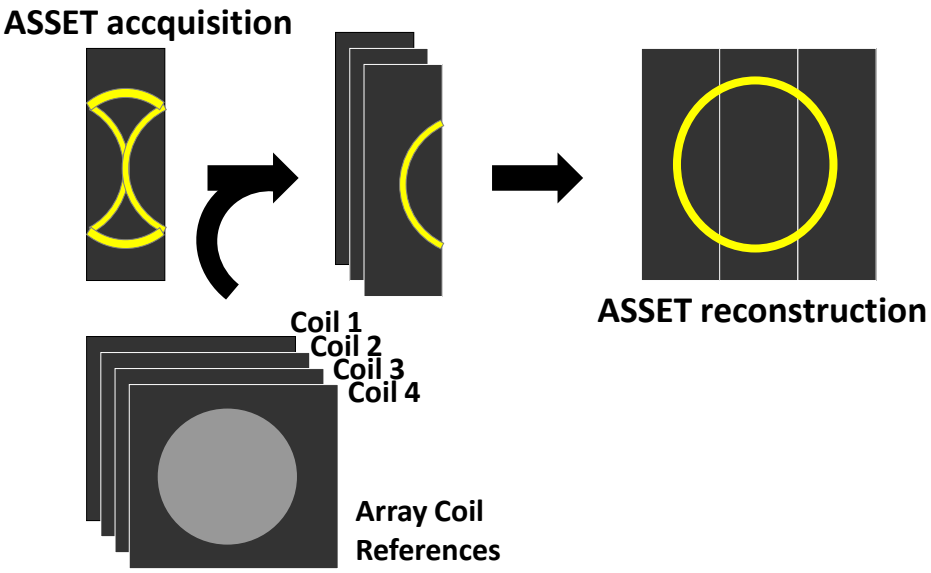

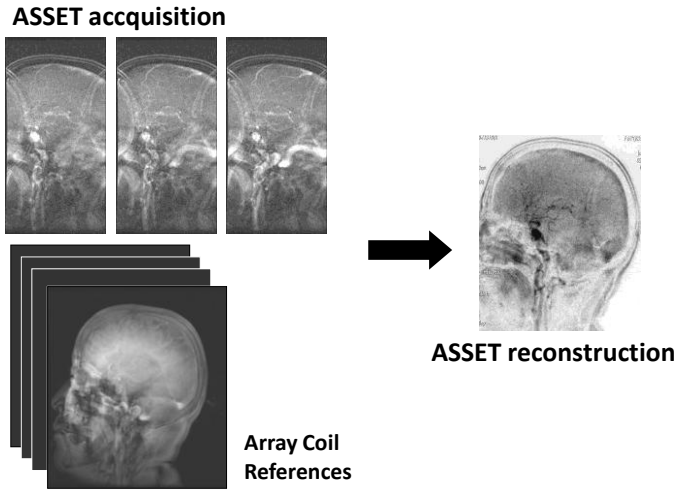

Appendix 3

Basic concepts of TRICKS

TRICKS imaging is performed by intensive data gathering from the low-frequency components that contribute to image contrast while selectively eliminating the high-frequency components that contribute to resolution. Use of these principles produces images with high temporal resolution that maintain high spatial resolution, and is applied to high-speed contrast 3D time resolved MRA.

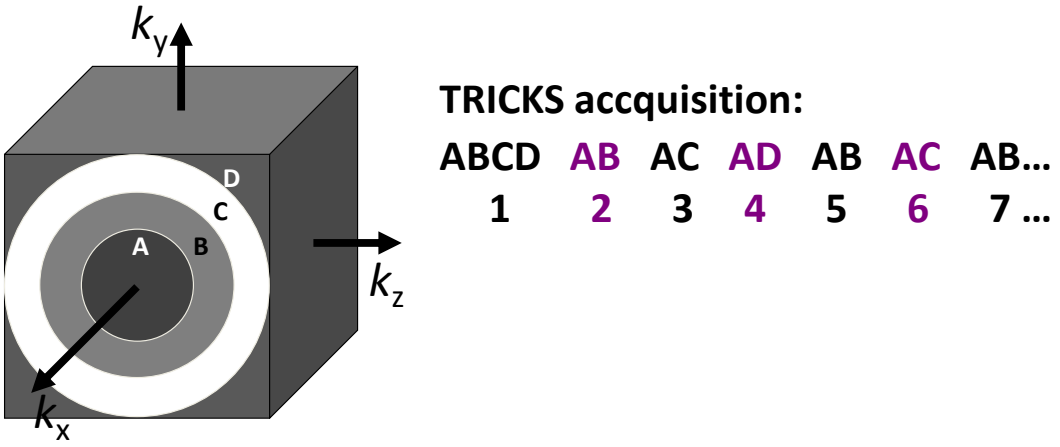

13. Acknowledgement

I would like to thank my fellow researchers Prof. Kuni Ohtomo (Department of Radiology, Graduate School and Faculty of Medicine, the University of Tokyo), Prof. Shigeki Aoki and Assoc. Prof. Masaaki Hori (Department of Radiology, Faculty of Medicine, Juntendo University), Assist. Prof. Kanako Kumamaru-Kunishima (Department of Radiology, Harvard Medical School, Brigham and Women's Hospital), Prof. Toshiyuki Okubo (Department of Radiology, Teikyo University Chiba Medical Center), Prof. Masao Tago (Department of Radiology, Teikyo University Mizonokuchi Hospital), Prof. Osamu Abe (Department of Radiology, Nihon University), Assoc. Prof. Naoto Hayashi and Assoc. Prof. Takeharu Yoshikawa (Department of Computational Diagnostic Radiology and Preventive Medicine, 22nd Century Medical and Research Center, the University of Tokyo), Assoc. Prof. Tomohiko Masumoto (Department of Intervention and Radiology, Graduate School of Comprehensive Human Sciences, University of Tsukuba), Prof. Hiroki Kurita and Assist. Prof. Tomoyuki Koga (Department of Neurosurgery, Saitama Medical University International Medical Center), Assist. Prof. Masahiro Shin (Department of Neurosurgery, Graduate School and Faculty of Medicine, the University of Tokyo), Assist. Prof. Keisuke Maruyama (Department of Neurosurgery, Kyorin University School of Medicine), Head Radiologist Daisuke Itoh (Department of Radiolgy, Nerima Hikarigaoka Hospital), and Ph. D. Hiroyuki Kabasawa (Applied Science Laboratory, GE Healthcare Japan) for their assistance and guidance in composing this paper. I express my sincere gratitude.

14. References

1. Adamis MK, Li W, Wielopolski PA, Kim D, Sax EJ, Kent KC, Edelman RR. Dynamic contrast-enhanced subtraction MR angiography of the lower extremities: initial evaluation with a multisection two-dimensional time-of-flight sequence. *Radiology*. 1995; 196(3):689-695.
2. Aoki S, Sasaki Y, Machida T, Hayashi N, Shirouzu I, Ohkubo T, Terahara A, Sasaki Y, Kawamoto S, Araki T, Maehara T. 3D-CT angiography of cerebral arteriovenous malformations. *Radiat Med*. 1998; 16(4):263-271.
3. Aoki S, Yoshikawa T, Hori M, Nanbu A, Kumagai H, Nishiyama Y, Nukui H, Araki T. MR digital subtraction angiography for the assessment of cranial arteriovenous malformations and fistulas. *AJR Am J Roentgenol*. 2000; 175(2):451-453.
4. Alley MT, Shifrin RY, Pelc NJ, Herfkens RJ. Ultrafast contrast-enhanced three-dimensional MR angiography: state of the art. *Radiographics*. 1998; 18(2):273-285.
5. Bendszus M, Koltzenburg M, Burger R, Warmuth-Metz M, Hofmann E, Solymosi L. Silent embolism in diagnostic cerebral angiography and neurointerventional procedures: a prospective study. *Lancet*. 1999; 354(9190):1594-1597.
6. Bosmans H, Marchal G, Lukito G, Yicheng N, Wilms G, Laub G, Baert AL. Time-of-flight MR angiography of the brain: comparison of acquisition techniques in healthy volunteers. *AJR Am J Roentgenol*. 1995; 164(1):161-167.
7. Campeau NG, Huston J 3rd, Bernstein MA, Lin C, Gibbs GF. Magnetic resonance angiography at 3.0 Tesla: initial clinical experience. *Top Magn Reson Imaging*. 2001; 12(3):183-204.
8. Cashen TA, Carr JC, Shin W, Walker MT, Futterer SF, Shaibani A, McCarthy RM,

Carroll TJ. Intracranial time-resolved contrast-enhanced MR angiography at 3T. *AJNR Am J Neuroradiol*. 2006; 27(4):822-829.

9. Chen JC, Tsuruda JS, Halbach VV. Suspected dural arteriovenous fistula: results with screening MR angiography in seven patients. *Radiology*. 1992; 183(1):265-271.
10. Chen Q, Quijano CV, Mai VM, Krishnamoorthy SK, Li W, Storey P, Edelman RR. On improving temporal and spatial resolution of 3D contrast-enhanced body MR angiography with parallel imaging. *Radiology*. 2004; 231(3):893-899.
11. Coffey RJ, Nichols DA, Shaw EG. Stereotactic radiosurgical treatment of cerebral arteriovenous malformations. Gamma Unit Radiosurgery Study Group. *Mayo Clin Proc*. 1995; 70(3):214-222.
12. Dawkins AA, Evans AL, Wattam J, Romanowski CA, Connolly DJ, Hodgson TJ, Coley SC. Complications of cerebral angiography: a prospective analysis of 2,924 consecutive procedures. *Neuroradiology*. 2007; 49(9):753-759.
13. De Marco JK, Nesbit GM, Wesbey GE, Richardson D. Prospective evaluation of extracranial carotid stenosis: MR angiography with maximum-intensity projections and multiplanar reformation compared with conventional angiography. *AJR Am J Roentgenol*. 1994; 163(5):1205-1212.
14. Douek PC, Revel D, Chazel S, Falise B, Villard J, Amiel M. Fast MR angiography of the aortoiliac arteries and arteries of the lower extremity: value of bolus-enhanced, whole-volume subtraction technique. *AJR Am J Roentgenol*. 1995; 165(2):431-437.
15. Duran M, Schoenberg SO, Yuh WT, Knopp MV, van Kaick G, Essig M. Cerebral arteriovenous malformations: morphologic evaluation by ultrashort 3D gadolinium-enhanced MR angiography. *Eur Radiol*. 2002; 12(12):2957-2964.
16. Farb RI, McGregor C, Kim JK, Laliberte M, Derbyshire JA, Willinsky RA, Cooper

PW, Westman DG, Cheung G, Schwartz ML, Stainsby JA, Wright GA. Intracranial arteriovenous malformations: real-time auto-triggered elliptic centric-ordered 3D gadolinium-enhanced MR angiography--initial assessment. *Radiology*. 2001;2220(1):244-251.

17. Fink C, Ley S, Kroeker R, Requardt M, Kauczor HU, Bock M. Time-resolved contrast-enhanced three-dimensional magnetic resonance angiography of the chest: combination of parallel imaging with view sharing (TREAT). *Invest Radiol*. 2005; 40(1):40-48.
18. Frayne R, Grist TM, Korosec FR, Willig DS, Swan JS, Turski PA, Mistretta CA. MR angiogaphy with three-dimensional MR digital subtraction angiography. *Top Magn Reson Imaging*. 1996; 8(6):366-388.
19. Gauvrit JY, Leclerc X, Oppenheim C, Munier T, Trystram D, Rachdi H, Nataf F, Pruvo JP, Meder JF. Three-dimensional dynamic MR digital subtraction angiography using sensitivity encoding for the evaluation of intracranial arteriovenous malformations: a preliminary study. *AJNR Am J Neuroradiol*. 2005; 26(6):1525-1531.
20. Gauvrit JY, Oppenheim C, Nataf F, Naggara O, Trystram D, Munier T, Fredy D, Pruvo JP, Roux FX, Leclerc X, Meder JF. Three-dimensional dynamic magnetic resonance angiography for the evaluation of radiosurgically treated cerebral arteriovenous malformations. *Eur Radiol*. 2006; 16(3):583-591.
21. Griffiths PD, Hoggard N, Warren DJ, Wilkinson ID, Anderson B, Romanowski CA. Brain arteriovenous malformations: assessment with dynamic MR digital subtraction angiography. *AJNR Am J Neuroradiol*. 2000; 21(10):1892-1899.
22. Guo WY. Application of MR in stereotactic radiosurgery. *J Magn Reson Imaging*. 1998; 8(2):415-420.

23. Heidenreich JO, Schilling AM, Unterharnscheidt F, Stendel R, Hartlieb S, Wacker FK, Schlattmann P, Wolf KJ, Bruhn H. Assessment of 3D-TOF-MRA at 3.0 Tesla in the characterization of the angioarchitecture of cerebral arteriovenous malformations: a preliminary study. *Acta Radiol*. 2007; 48(6):678-686.

24. Heiserman JE, Dean BL, Hodak JA, Flom RA, Bird CR, Drayer BP, Fram EK. Neurologic complications of cerebral angiography. *AJNR Am J Neuroradiol*. 1994; 15(8):1401-1407.

25. Hendrick RE, Roff U. Image contrast and noise. In: Stark DD, Bradley WG, eds. Magnetic resonance imaging. Chicago, I11: Mosby-Year Book, 1991; p135.

26. Hennig J, Scheffler K, Laubenberger J, Strecker R. Time-resolved projection angiography after bolus injection of contrast agent. *Magn Reson Med*. 1997; 37(3):341-345.

27. Holland GA, Dougherty L, Carpenter JP, Golden MA, Gilfeather M, Slossman F, Schnall MD, Axel L. Breath-hold ultrafast three-dimensional gadolinium-enhanced MR angiography of the aorta and the renal and other visceral abdominal arteries. *AJR Am J Roentgenol*. 1996; 166(4):971-981.

28. Ingmar Wickbom. Tumor circulation. In: Newton TH, Potts DG (ed) Radiology of the skull and brain angiography. The C. V. Mosby Company, Saint Louis, 1974; pp2257-2285.

29. Jung HW, Chang KH, Choi DS, Han MH, Han MC. Contrast-enhanced MR angiography for the diagnosis of intracranial vascular disease: optimal dose of gadopentetate dimeglumine. *AJR Am J Roentgenol*. 1995; 165(5):1251-1255.

30. Kallmes DF, Cloft HJ, Jensen ME, Kaptain GJ, Dion JE, Matsumoto JA. Dural arteriovenous fistula: a pitfall of time-of-flight MR venography for the diagnosis of

sinus thrombosis. *Neuroradiology*. 1998; 40(4):242-4.

31. Kauczor HU, Engenhart R, Layer G, Gamroth AH, Wowra B, Schad LR, Semmler W, van Kaick G. 3D TOF MR angiography of cerebral arteriovenous malformations after radiosurgery. *J Comput Assist Tomogr*. 1993; 17(2):184-190.
32. Klisch J, Strecker R, Hennig J, Schumacher M. Time-resolved projection MRA: clinical application in intracranial vascular malformations. *Neuroradiology*. 2000; 42(2):104-107.
33. Korosec FR, Frayne R, Grist TM, Mistretta CA. Time-resolved contrast-enhanced 3D MR angiography. *Magn Reson Med*. 1996; 36(3):345-351.
34. Kuntz KM, Skillman JJ, Whittemore AD, Kent KC. Carotid endarterectomy in asymptomatic patients--is contrast angiography necessary? A morbidity analysis. *J Vasc Surg*. 1995;22(6):706-14
35. Lee HM, Wang Y, Sostman HD, Schwartz LH, Khilnani NM, Trost DW, Ramirez de Arellano E, Teeger S, Bush HL Jr. Distal lower extremity arteries: evaluation with two-dimensional MR digital subtraction angiography. *Radiology*. 1998;207(2):505-512.
36. Leung DA, McKinnon GC, Davis CP, Pfammatter T, Krestin GP, Debatin JF. Breath-hold, contrast-enhanced, three-dimensional MR angiography. *Radiology*. 1996; 200(2):569-571.
37. Madore B, Pelc NJ. New approach to 3D time-resolved angiography. *Magn Reson Med*. 2002;47(5):1022-1025.
38. Marchal G, Bosmans H, Van Fraeyenhoven L, Wilms G, Van Hecke P, Plets C, Baert AL. Intracranial vascular lesions: optimization and clinical evaluation of three-dimensional time-of-flight MR angiography. *Radiology*. 1990; 175(2):443-448.

39. Marchal G, Michiels J, Bosmans H, Van Hecke P. Contrast-enhanced MRA of the brain. *J Comput Assist Tomogr*. 1992; 16(1):25-29.

40. Maruyama K, Kawahara N, Shin M, Tago M, Kishimoto J, Kurita H, Kawamoto S, Morita A, Kirino T. The risk of hemorrhage after radiosurgery for cerebral arteriovenous malformations. *N Engl J Med*. 2005; 352(2):146-153.

41. Masaryk TJ, Modic MT, Ross JS, Ruggieri PM, Laub GA, Lenz GW, Haacke EM, Selman WR, Wiznitzer M, Harik SI. Intracranial circulation: preliminary clinical results with three-dimensional (volume) MR angiography. *Radiology*. 1989; 171(3):793-799.

42. Mazaheri Y, Carroll TJ, Du J, Block WF, Fain SB, Hany TF, Aagaard BD, Strother CM, Mistretta CA, Grist TM. Combined time-resolved and high-spatial-resolution 3D MRA using an extended adaptive acquisition. *J Magn Reson Imaging*. 2002; 15(3):291-301.

43. Meckel S, Maier M, Ruiz DS, Yilmaz H, Scheffler K, Radue EW, Wetzel SG. MR angiography of dural arteriovenous fistulas: diagnosis and follow-up after treatment using a time-resolved 3D contrast-enhanced technique. *AJNR Am J Neuroradiol*. 2007; 28(5):877-884.

44. Meder JF, Oppenheim C, Blustajn J, Nataf F, Merienne L, Lefkoupolos D, Laurent A, Merland JJ, Schlienger M, Fredy D. Cerebral arteriovenous malformations: the value of radiologic parameters in predicting response to radiosurgery. *AJNR Am J Neuroradiol*. 1997; 18(8):1473-1483.

45. Mori H, Aoki S, Okubo T, Hayashi N, Masumoto T, Yoshikawa T, Tago M, Shin M, Kurita H, Abe O, Ohtomo K. Two-dimensional thick-slice MR digital subtraction angiography in the assessment of small to medium-size intracranial arteriovenous

malformations. *Neuroradiology*. 2003; 45(1):27-33.

46. Nussel F, Wegmuller H, Huber P. Comparison of magnetic resonance angiography, magnetic resonance imaging and conventional angiography in cerebral arteriovenous malformation. *Neuroradiology*. 1991; 33(1):56-61.

47. Oppenheim C, Meder JF, Trystram D, Nataf F, Godon-Hardy S, Blustajn J, Merienne L, Schlienger M, Fredy D. Radiosurgery of cerebral arteriovenous malformations: is an early angiogram needed? *AJNR Am J Neuroradiol*. 1999; 20(3):475-481.

48. Osborn AG (ed). Diagnostic cerebral angiography, second edition, Lippincott Williams & Wilkins, Philadelphia, 1998; pp313-340.

49. Peggy W, William W. MRI optimization. McGraw-Hill co., Inc., 1998.

50. Pollock BE, Kondziolka D, Flickinger JC, Patel AK, Bissonette DJ, Lunsford LD. Magnetic resonance imaging: an accurate method to evaluate arteriovenous malformations after stereotactic radiosurgery. *J Neurosurg*. 1996; 85(6):1044-1049.

51. Prince MR. Gadolinium-enhanced MR aortography. *Radiology*. 1994; 191(1):155-164.

52. Prince MR, Chenevert TL, Foo TK, Londy FJ, Ward JS, Maki JH. Contrast-enhanced abdominal MR angiography: optimization of imaging delay time by automating the detection of contrast material arrival in the aorta. *Radiology*. 1997; 203(1):109-114.

53. Prince MR, Yucel EK, Kaufman JA, Harrison DC, Geller SC. Dynamic gadolinium-enhanced three-dimensional abdominal MR arteriography. *J Magn Reson Imaging*. 1993; 3(6):877-881.

54. Pruessmann KP, Weiger M, Scheidegger MB, Boesiger P. SENSE: sensitivity

encoding for fast MRI. *Magn Reson Med*. 1999; 42(5):952-962.

55. Remonda L, Heid O, Schrogh G. Carotid artery stenosis, occlusion, and pseudo-occlusion: first-pass, gadolinium-enhanced, three-dimensional MR angiography--preliminary study. *Radiology*. 1998; 209(1):95-102.

56. Rempp KA, Brix G, Wenz F, Becker CR, Guckel F, Lorenz WJ. Quantification of regional cerebral blood flow and volume with dynamic susceptibility contrast-enhanced MR imaging. *Radiology*. 1994; 193(3):637-641.

57. Revel D, Loubeyre P, Delignette A, Douek P, Amiel M. Contrast-enhanced magnetic resonance tomoangiography: a new imaging technique for studying thoracic great vessels. *Magn Reson Imaging*. 1993; 11(8):1101-1105.

58. Scarabino T, Popolizio T, Giannatempo GM, Nemore F, Maiorana A, Carriero A, Messana D, Maggialetti A, Armillotta M, Salvolini U. 3.0-T morphological and angiographic brain imaging: a 5-years experience. *Radiol Med*. 2007; 112(1):82-96.

59. Shetty AN, Bis KG, Vrachliotis TG, Kirsch M, Shirkhoda A, Ellwood R. Contrast-enhanced 3D MRA with centric ordering in k space: a preliminary clinical experience in imaging the abdominal aorta and renal and peripheral arterial vasculature. *J Magn Reson Imaging*. 1998; 8(3):603-615.

60. Slosman F, Stolpen AH, Lexa FJ, Schnall MD, Langlotz CP, Carpenter JP, Goldberg HI. Extracranial atherosclerotic carotid artery disease: evaluation of non-breath-hold three-dimensional gadolinium-enhanced MR angiography. *AJR Am J Roentgenol*. 1998; 170(2):489-495.

61. Snidow JJ, Johnson MS, Harris VJ, Margosian PM, Aisen AM, Lalka SG, Cikrit DF, Trerotola SO. Three-dimensional gadolinium-enhanced MR angiography for aortoiliac inflow assessment plus renal artery screening in a single breath hold. *Radiology*. 1996;

198(3):725-732.

62. Sorensen AG, Buonanno FS, Gonzalez RG, Schwamm LH, Lev MH, Huang-Hellinger FR, Reese TG, Weisskoff RM, Davis TL, Suwanwela N, Can U, Moreira JA, Copen WA, Look RB, Finklestein SP, Rosen BR, Koroshetz WJ. Hyperacute stroke: evaluation with combined multisection diffusion-weighted and hemodynamically weighted echo-planar MR imaging. *Radiology*. 1996; 199(2):391-401.

63. Spetzler RF, Martin NA. A proposed grading system for arteriovenous malformations. *J Neurosurg.* 1986; 65(4):476-483.

64. Stehling MK, Niedermeyer M, Laub G. Contrast-enhanced magnetic resonance angiography. Theory, technique and practical application. *Radiologe*. 1997; 37(7):501-507.

65. Stock KW, Radue EW, Jacob AL, Bao XS, Steinbrich W. Intracranial arteries: prospective blinded comparative study of MR angiography and DSA in 50 patients. *Radiology*. 1995; 195(2):451-456.

66. Summers PE, Kollias SS, Valavanis A. Resolution improvement in thick-slab magnetic resonance digital subtraction angiography using SENSE at 3T. *J Magn Reson Imaging*. 2004; 20(4):662-673.

67. Todaka T, Hamada J, Kai Y, Morioka M, Ushio Y. Analysis of mean transit time of contrast medium in ruptured and unruptured arteriovenous malformations: a digital subtraction angiographic study. *Stroke*. 2003; 34(10):2410-2414.

68. Tsuchiya K, Katase S, Yoshino A, Hachiya J. MR digital subtraction angiography of cerebral arteriovenous malformations. *AJNR Am J Neuroradiol*. 2000; 21(4):707-711.

69. Turski PA, Korosec FR, Carroll TJ, Willig DS, Grist TM, Mistretta CA.

Contrast-Enhanced magnetic resonance angiography of the carotid bifurcation using the time-resolved imaging of contrast kinetics (TRICKS) technique. *Top Magn Reson Imaging*. 2001; 12(3):175-181.

70. Unlu E, Temizoz O, Albayram S, Genchellac H, Hamamcioglu MK, Kurt I, Demir MK. Contrast-enhanced MR 3D angiography in the assessment of brain AVMs. *Eur J Radiol*. 2006; 60(3):367-378.

71. Wang Y, Johnston DL, Breen JF, Huston J 3rd, Jack CR, Julsrud PR, Kiely MJ, King BF, Riederer SL, Ehman RL. Dynamic MR digital subtraction angiography using contrast enhancement, fast data acquisition, and complex subtraction. *Magn Reson Med*. 1996; 36(4):551-556.

72. Warach S, Dashe JF, Edelman RR. Clinical outcome in ischemic stroke predicted by early diffusion-weighted and perfusion magnetic resonance imaging: a preliminary analysis. *J Cereb Blood Flow Metab*. 1996; 16(1):53-9.

73. Warren DJ, Hoggard N, Walton L, Radatz MW, Kemeny AA, Forster DM, Wilkinson ID, Griffiths PD. Cerebral arteriovenous malformations: comparison of novel magnetic resonance angiographic techniques and conventional catheter angiography. *Neurosurgery*. 2001; 48(5):973-982.

74. Weiger M, Pruessmann KP, Boesiger P. Cardiac real-time imaging using SENSE. SENSitivity Encoding scheme. *Magn Reson Med*. 2000; 43(2):177-184.

75. Weiger M, Pruessmann KP, Kassner A, Roditi G, Lawton T, Reid A, Boesiger P. Contrast-enhanced 3D MRA using SENSE. *J Magn Reson Imaging*. 2000; 12(5):671-677.

76. Wilcock DJ, Jaspan T, Worthington BS. Problems and pitfalls of 3-D TOF magnetic resonance angiography of the intracranial circulation. *Clin Radiol*. 1995;

50(8):526-532.

77. Willig DS, Turski PA, Frayne R, Graves VB, Korosec FR, Swan JS, Mistretta CA, Grist TM. Contrast-enhanced 3D MR DSA of the carotid artery bifurcation: preliminary study of comparison with unenhanced 2D and 3D time-of-flight MR angiography. *Radiology*. 1998; 208(2):447-451.

78. Wilman AH, Riederer SJ, Huston J 3rd, Wald JT, Debbins JP. Arterial phase carotid and vertebral artery imaging in 3D contrast-enhanced MR angiography by combining fluoroscopic triggering with an elliptical centric acquisition order. *Magn Reson Med*. 1998; 40(1):24-35.

79. Yamashita Y, Mitsuzaki K, Ogata I, Takahashi M, Hiai Y. Three-dimensional high-resolution dynamic contrast-enhanced MR angiography of the pelvis and lower extremities with use of a phased array coil and subtraction: diagnostic accuracy. *J Magn Reson Imaging*. 1998; 8(5):1066-1072.

80. Yoshikawa T, Aoki S, Hori M, Nambu A, Kumagai H, Araki T. Time-resolved two-dimensional thick-slice magnetic resonance digital subtraction angiography in assessing brain tumors. *Eur Radiol*. 2000; 10(5):736-744.